

Total energy partitioning within a one-electron formalism: A Hamilton population study of surface-CO interaction in the $c(2\times 2)$ -CO/Ni(100) chemisorption system

Wingfield V. Glassey, Garegin A. Papoian, and Roald Hoffmann^{a)}

Department of Chemistry and Chemical Biology, Cornell University, Ithaca, New York 14853-1301

(Received 28 December 1998; accepted 6 April 1999)

A scheme for total electronic energy partitioning within the framework of a one-electron theory of the extended Hückel-type is presented, with a view to extending and augmenting the capabilities of existing theoretical electronic structure analysis tools, specifically overlap population analysis. A total electronic energy partitioning is developed first for molecular and subsequently extended materials. In constructing the partitioning, we define molecular orbital Hamilton populations (MOHP's) for discrete systems, and Crystal Orbital Hamilton Populations (COHP's) for extended systems. The various energy partitionings and overlap population analyses are exemplified and contrasted for HX (X=F,Cl,Br), ethane, and a $[\text{PtH}_4]^{2-}$ polymer. The utility of energy partitioning is demonstrated by effecting a COHP partitioning of the surface-CO interaction for the $c(2\times 2)$ -CO/Ni(100) chemisorption system. Aspects of the surface-CO interaction less amenable to overlap population analysis are addressed, specifically the role of energetically low-lying filled CO orbitals and the relative contributions of surface s , p , and d bands to surface-CO interaction. Hamilton population analysis leads to a CO (4σ , 5σ)-metal forward donation, metal-CO ($2\pi^*$) backdonation model for the surface-CO interaction. The metal σ contribution to surface-CO bonding is described as sp dominated metal spd hybrid-CO bonding, modifying slightly the metal d -CO σ bonding model proposed by Blyholder. The metal $d-2\pi^*$ backdonation of the Blyholder model remains. The role of the CO(1π) orbitals is also discussed in the context of CO orbital mixing on binding CO to the Ni(100) surface. © 1999 American Institute of Physics. [S0021-9606(99)30325-1]

I. INTRODUCTION

Most of the electronic energy of a molecule resides within the individual atoms, the contribution arising from bonding interactions between atoms accounting for typically, a few percent of the total electronic energy of the system. Yet bonding between atoms remains the focus of attention for chemists, materials scientists, and physicists alike.

The goals of the present study are (1) The development of a theoretical framework for total energy partitioning in extended materials, based on a simple tight binding model of the extended Hückel-type. The approach adopted closely parallels that presented previously by Dronskowski and Blöchl¹ within a density functional theory framework; (2) To understand how energy partitioning and overlap population analysis of electron distribution are related and to examine the extent to which energy partitioning can augment the capabilities of overlap population analysis.

The energy partitioning formalism developed in this work for extended systems permits localization, in direct space, of orbital interactions. Orbital interactions within the unit cell and between unit cells become separable — a feature not inherent in previous energy partitioning schemes for extended materials.¹ Thus it is possible to address the validity of surface-molecule bonding analogies such as that pre-

sented in this and previous work for Ni-CO interaction in molecular $[\text{H}_5\text{NiCO}]^-$ and CO chemisorbed “on-top” on a Ni(100) surface.²

We begin by reformulating the molecular energy partitioning scheme derived by Dronskowski³ within an extended Hückel framework. We define the molecular orbital Hamilton population (MOHP) — the discrete analog of the term crystal orbital Hamilton population (COHP) introduced previously by Dronskowski and Blöchl.¹ The valence orbital based MOHP formulation is then recast into energy partitioning schemes based on atomic contributions — the analog of the one- and two-center or “atom-bond” partitioning developed by Pople *et al.* within a CNDO framework,⁴ and molecular fragment energy contributions.

Both atom-based “atom-bond” and molecular fragment-based energy partitionings are chemically intuitive. Molecular fragment based energy partitioning schemes embrace the “functional group” concept of reactivity in allowing electronic structure changes resulting from a structural change to be localized in one or more molecular fragments.

We proceed by deriving extended structure analogs of the orbital, atom, and fragment based energy partitionings presented for molecular systems and conclude the theoretical section with a discussion on the utility of energy partitioning with fragment orbital basis sets. Applications to chemical bonding in discrete and extended systems are interspersed with the theory. As an illustration of the unique capabilities of this new analytical tool, we examine aspects of Ni-CO

^{a)} Author to whom correspondence should be addressed. Electronic mail: rh34@cornell.edu

interaction for the prototypical, and well characterized, CO-transition metal chemisorption system $c(2 \times 2)$ -CO/Ni(100).⁵⁻¹⁴

II. TOTAL ELECTRONIC ENERGY PARTITIONING IN MOLECULAR SYSTEMS

Consider a one-electron effective Hamiltonian formalism, such as the extended Hückel method.^{15,16} For a valence orbital basis $\{\phi_\nu\}$ within the LCAO approximation the wavefunctions (molecular orbitals) ψ_i are given by

$$\psi_i = \sum_\nu c_{\nu i} \phi_\nu, \text{ where } \langle \phi_\nu | \phi_\nu \rangle = 1 \text{ for all } \nu. \quad (1)$$

The i th eigenvalue for the system is

$$E_i = \langle \psi_i | \hat{H} | \psi_i \rangle, \quad (2)$$

and the total electronic energy, E_{tot} for the molecular system is given by Eq. (3) for a set of molecular orbital occupations $\{n_i\}$,

$$E_{\text{tot}} = \sum_{\text{MO's } i} n_i E_i. \quad (3)$$

The total molecular electronic energy can be expressed as a sum over Hamiltonian matrix elements (see, for example, Ref. 17). Substituting Eqs. (1) and (2) in Eq. (3) gives

$$E_{\text{tot}} = \sum_{\text{MO's } i} n_i \left\{ \sum_\mu |c_{\mu i}|^2 \mathbf{H}_{\mu\mu} + \sum_\mu \sum_{\nu \neq \mu} c_{\mu i}^* c_{\nu i} \mathbf{H}_{\mu\nu} \right\}, \quad (4)$$

where $\langle \phi_\mu | \hat{H} | \phi_\nu \rangle = \mathbf{H}_{\mu\nu} = \mathbf{H}_{\nu\mu}^*$.

Equation (4) is an energy partitioning. It is constructive to identify terms in Eq. (4) as "on-site" and "off-site" total energy contributions, as defined by Dronskowski and Blöchl.¹ Equations (5) and (6) define, respectively, the on-site total energy contribution for the μ th basis function, to be called hereafter $\text{MOHP}_{\mu\mu}$ and the off-site total energy contribution for the μ th and ν th basis functions, $\text{MOHP}_{\mu\nu}$. The term Molecular Orbital Hamilton Population (MOHP) is here introduced as the molecular analogue of Dronskowski and Blöchl's Crystal Orbital Hamilton Population (COHP) for extended systems,¹

$$\text{MOHP}_{\mu\mu} = \sum_{\text{MO's } i} n_i |c_{\mu i}|^2 \mathbf{H}_{\mu\mu}, \quad (5)$$

$$\text{MOHP}_{\mu\nu} = \sum_{\text{MO's } i} n_i \{ c_{\mu i}^* c_{\nu i} \mathbf{H}_{\mu\nu} + c_{\mu i} c_{\nu i}^* \mathbf{H}_{\nu\mu} \}. \quad (6)$$

The electronic energy (4) can be written as a sum over on-site and off-site MOHP's as follows:

$$E_{\text{tot}} = \sum_\mu \text{MOHP}_{\mu\mu} + \frac{1}{2} \sum_\mu \sum_{\nu \neq \mu} \text{MOHP}_{\mu\nu}. \quad (7)$$

In obtaining Eq. (7) a specific form for the molecular Hamiltonian has not been invoked. Thus the energy decomposition scheme is applicable to all theoretical methods utilizing an atom localized basis set, and a one-electron formalism.

III. MOLECULAR HAMILTON POPULATIONS: AN EXTENDED HÜCKEL APPROACH

Having just presented a somewhat general theoretical framework for total electronic energy analysis in molecular systems, it proves useful to consider the total electronic energy analysis scheme in the context of the extended Hückel model. Given the familiar Wolfsberg-Helmholtz approximation of $\mathbf{H}_{\mu\nu}$,¹⁸

$$\mathbf{H}_{\mu\nu} = \frac{\kappa}{2} (\mathbf{H}_{\mu\mu} + \mathbf{H}_{\nu\nu}) \mathbf{S}_{\mu\nu} = \kappa_{\mu\nu} \mathbf{S}_{\mu\nu},$$

where

$$\mathbf{S}_{\mu\nu} = \langle \phi_\mu | \phi_\nu \rangle \text{ and } \kappa = 1.75. \quad (8)$$

Equations (5) and (6) can be rewritten as

$$\text{MOHP}_{\mu\mu} = \sum_{\text{MO's } i} n_i |c_{\mu i}|^2 \mathbf{H}_{\mu\mu}, \quad (9)$$

$$\text{MOHP}_{\mu\nu} = \sum_{\text{MO's } i} 2 n_i c_{\mu i} c_{\nu i} \kappa_{\mu\nu} \mathbf{S}_{\mu\nu}. \quad (10)$$

There is in common another use of the Wolfsberg-Helmholtz relationship, introduced to counteract the effects of counterintuitive orbital mixing,^{19,20} the argument and the analytical tools devised in this paper are not affected by this modification.

It is seen that the on- and off-site MOHP's, Eqs. (9) and (10) respectively, are intimately related to the corresponding on- and off-site Mulliken overlap population's (MOOP's) (Refs. 16 and 21) defined by Eqs. (11) and (12), respectively,

$$\text{MOOP}_{\mu\mu} = \sum_{\text{MO's } i} n_i |c_{\mu i}|^2, \quad (11)$$

$$\text{MOOP}_{\mu\nu} = \sum_{\text{MO's } i} 2 n_i c_{\mu i} c_{\nu i} \mathbf{S}_{\mu\nu}. \quad (12)$$

Overlap populations can be used, as in the case of Mulliken population analysis, to partition the electron distribution,

$$\sum_\mu \text{MOOP}_{\mu\mu} + \frac{1}{2} \sum_\mu \sum_{\nu \neq \mu} \text{MOOP}_{\mu\nu} = N, \quad (13)$$

where N denotes the total number of electrons in the system.

IV. MOHP ANALYSIS OF THE HYDROGEN HALIDES, HX (X=F, Cl, Br)

MOOP analysis provides a measure of on- and off-site electron distribution within a molecule. MOHP studies based on the energy partitioning (7) may complement and enhance chemical interpretation of MOOP analyses of electron distribution. Consider, for example, bonding in the series of hydrogen halides HX (X=F, Cl, Br). The extended Hückel parameters and HX bond lengths used in the calculations are given in the Appendix.

One point of interest when considering bonding in the hydrogen halides is the relative contribution of the halogen s

TABLE I. Comparative OP and HP analyses of halogen s and p contributions to HX bonding for X=F, Cl, Br. The percent contribution of X(p)-H interactions is given in parentheses.

HF	F(s)-H	F(p)-H	Total
OP	0.247	0.256 [51]	0.503
HP/eV	-12.91	-7.19 [36]	-20.10
HCl	Cl(s)-H	Cl(p)-H	Total
OP	0.175	0.558 [76]	0.733
HP/eV	-6.45	-13.58 [68]	-20.03
HBr	Br(s)-H	Br(p)-H	Total
OP	0.131	0.563 [81]	0.694
HP/eV	-3.66	-12.96 [78]	-16.62

and p orbitals. Comparative MOOP and MOHP analyses of HX bonding are given in Table I. It is important to remember that, in general, negative Hamilton populations correspond to stabilizing interactions in contrast to the destabilization inferred by a negative overlap population. This “inverse” relation in sign between Mulliken overlap populations and the corresponding Hamilton populations is clearly illustrated in Table I.

Fluorine offers the most striking contrast between the results of MOOP and MOHP analyses. MOOP analysis places approximately equal importance on F(s)-H and F(p)-H interactions, whereas MOHP analysis shows that approximately $\frac{2}{3}$ of the energy of interaction may be attributed to F(s)-H interaction.

As can be seen from Table I, the discrepancy between MOOP and MOHP descriptions of HX interaction is substantially reduced for HCl and still further reduced for HBr. The convergence of the MOOP and MOHP descriptions of HX bonding on going from HF to HBr may be understood by considering MOHP analysis to be an “energy-weighted” MOOP analysis. The off-site MOHP and MOOP definitions, Eqs. (10) and (12), respectively, differ only in the factor $\kappa_{\mu\nu}$ as defined by Eq. (8). The “energy weight” $\kappa_{\mu\nu}$ increases linearly with increasing $\mathbf{H}_{\mu\mu}$ and $\mathbf{H}_{\nu\nu}$ — the diagonal Hamiltonian matrix elements, \mathbf{H}_{ii} being related to the valence shell ionization potential (VSIP) for the i th atomic (valence) orbital. Hence the difference between $\kappa_{\text{HX}(s)}$ and $\kappa_{\text{HX}(p)}$ decreases on going from HF to HBr, as does the discrepancy in the ratio of H-X(s) and H-X(p) contributions to HX binding. Figure 1 illustrates graphically (by contrasting the extremes of X=F, Br) the interactions in these HX systems, and the very different energies of the F and Br orbitals.

We argue that when one is dealing with heteronuclear or homonuclear interactions involving two or more valence basis function types (s, p, d, f) with widely separated \mathbf{H}_{ii} 's on a particular atomic center, an energy based MOHP analysis becomes the preferred option over a MOOP analysis of electron distribution.

V. IMPLEMENTING TOTAL ELECTRONIC ENERGY ANALYSIS IN MOLECULES: AN EXTENDED HÜCKEL APPROACH

The total electronic energy decomposition scheme (7) allows for evaluation of orbital-by-orbital contributions to

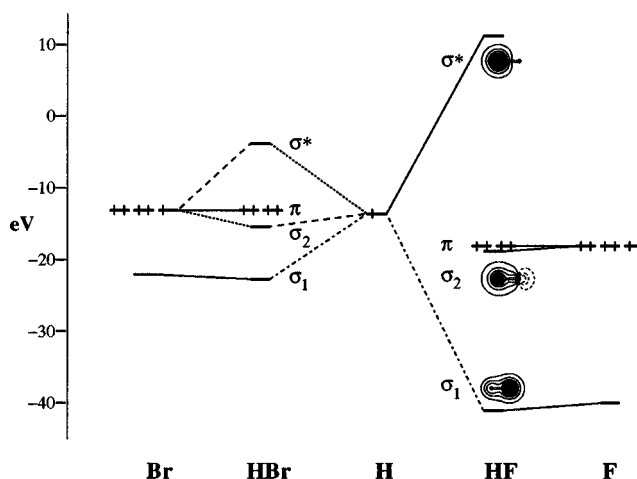


FIG. 1. Molecular orbital diagrams for HBr and HF.

the total electronic energy of a molecule. Such a scheme does not immediately lend itself to a bond-by-bond analysis of electronic structure — perhaps the most chemically intuitive total energy decomposition scheme. With this goal in mind the following atom- and bond-based scheme is proposed.

Consider a molecular system for which the valence basis associated with the i th atom is defined by the set of orbitals $\mathcal{A}^{(i)}$. Equation (7) becomes

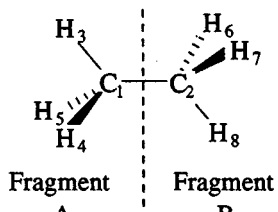
$$\begin{aligned}
 E_{\text{tot}} = & \sum_i \sum_{\mu \in \mathcal{A}^{(i)}} \text{MOHP}_{\mu\mu} \\
 & + \frac{1}{2} \sum_i \sum_{\mu \in \mathcal{A}^{(i)}} \sum_{\substack{\nu \in \mathcal{A}^{(i)} \\ \nu \neq \mu}} \text{MOHP}_{\mu\nu} \\
 & + \frac{1}{2} \sum_i \sum_{\substack{\text{ATOMS} \\ j \neq i}} \sum_{\mu \in \mathcal{A}^{(i)}} \sum_{\nu \in \mathcal{A}^{(j)}} \text{MOHP}_{\mu\nu}. \quad (14)
 \end{aligned}$$

For an orthogonal valence basis on each atomic center, Eq. (14) can be simplified to yield Eq. (15) — the MOHP's between different valence basis functions on the same atomic center being equal to zero,

$$\begin{aligned}
 E_{\text{tot}} = & \sum_i \sum_{\mu \in \mathcal{A}^{(i)}} \text{MOHP}_{\mu\mu} \\
 & + \frac{1}{2} \sum_i \sum_{\substack{\text{ATOMS} \\ j \neq i}} \sum_{\mu \in \mathcal{A}^{(i)}} \sum_{\nu \in \mathcal{A}^{(j)}} \text{MOHP}_{\mu\nu}. \quad (15)
 \end{aligned}$$

Equation (15) can be expressed in terms of on- and off-site atomic Hamilton populations as defined by Eqs. (16) and (17), respectively,

TABLE II. AHP analysis for ethane. Symmetry equivalent AHP's have been omitted.



ATOM contributions			
Atom	AHP/eV		
C	-37.26		
H	-8.87		
BOND contributions			
Between atoms	AHP/eV	Between atoms	AHP/eV
C ₁ -C ₂	-19.23	H ₃ -H ₄	1.03
C ₁ -H ₃	-19.44	H ₃ -H ₆	0.12
C ₁ -H ₆	1.16	H ₃ -H ₈	-0.06

$$\text{AHP}_i = \sum_{\mu \in A^{(i)}} \text{MOHP}_{\mu\mu}, \quad (16)$$

$$\text{AHP}_{ij} = \sum_{\mu \in A^{(i)}} \sum_{\nu \in A^{(j)}} \text{MOHP}_{\mu\nu}. \quad (17)$$

Thus the total electronic energy can be written as

$$\mathbf{E}_{\text{tot}} = \sum_{\text{ATOMS}} \text{AHP}_i + \frac{1}{2} \sum_{\text{ATOMS}} \sum_{\text{ATOMS}} \sum_{j \neq i} \text{AHP}_{ij}. \quad (18)$$

Equation (18) enables electronic energy distributions within molecular systems to be analyzed efficiently. For molecular systems containing large numbers of atoms, the atom by atom energy decomposition scheme (18) provides an economical scheme for localizing and highlighting electronic features of interest.

The atom based scheme (18) can be recast in a form based on molecular fragments — a fragment being simply defined as a subset of all atoms in the molecule. Equation (19) gives the total electronic energy as a sum over intra- and inter-fragment Hamilton populations, as defined by Eqs. (20) and (21), respectively. The set $\mathcal{B}^{(m)}$ contains the atoms belonging to the m th fragment as elements

$$\mathbf{E}_{\text{tot}} = \sum_{\text{FRAGS}} \text{FHP}_m + \frac{1}{2} \sum_{\text{FRAGS}} \sum_{\text{FRAGS}} \sum_{n \neq m} \text{FHP}_{mn}, \quad (19)$$

$$\text{FHP}_m = \sum_{\text{ATOMS}} \text{AHP}_i + \frac{1}{2} \sum_{\text{ATOMS}} \sum_{\text{ATOMS}} \sum_{\substack{j \in \mathcal{B}^{(m)} \\ j \neq i}} \text{AHP}_{ij}, \quad (20)$$

$$\text{FHP}_{mn} = \sum_{\text{ATOMS}} \sum_{\text{ATOMS}} \sum_{\substack{i \in \mathcal{B}^{(m)} \\ j \in \mathcal{B}^{(n)}}} \text{AHP}_{ij}. \quad (21)$$

VI. FRAGMENT ENERGY PARTITIONING IN ETHANE

At this point in the discussion it is instructive to effect a total energy partitioning for a simple molecule such as ethane. Table II summarizes an AHP analysis of ethane. The on- and off-site AHP's, as defined by Eqs. (16) and (17), respectively, are equivalently referred to as "atom" and "bond" energy contributions.

The total "atom" and "bond" contributions to the total electronic energy of ethane, as calculated within the extended Hückel approximation, are given by Eqs. (22) and (23), respectively

$$\begin{aligned} \text{atom contribution} &= \sum_{\text{ATOMS}} \text{AHP}_i = 2 \text{AHP}_1 + 6 \text{AHP}_3 \\ &= -127.74 \text{ eV}, \quad (22) \end{aligned}$$

$$\begin{aligned} \text{bond contribution} &= \frac{1}{2} \sum_{\text{ATOMS}} \sum_{\substack{\text{ATOMS} \\ j \neq i}} \text{AHP}_{ij} \\ &= \text{AHP}_{12} + 6 \text{AHP}_{13} + 6 \text{AHP}_{16} \\ &\quad + 6 \text{AHP}_{34} + 6 \text{AHP}_{36} + 3 \text{AHP}_{38} \\ &= -122.19 \text{ eV}. \quad (23) \end{aligned}$$

Ethane can be partitioned into two CH_3 fragments **A** and **B** as shown in Table II, the total electronic energy being composed of the individual intrafragment FHP's for the CH_3 units, FHP_A and FHP_B , and an interfragment FHP between the two CH_3 units, FHP_{AB} . The FHP's can, according to Eqs. (20) and (21), be expressed in terms of AHP's and are written,

$$\begin{aligned} \text{FHP}_A = \text{FHP}_B &= \text{AHP}_1 + 3 \text{AHP}_3 + 3 \text{AHP}_{13} + 3 \text{AHP}_{34} \\ &= -119.1 \text{ eV}, \quad (24) \end{aligned}$$

and

$$\begin{aligned} \text{FHP}_{AB} &= \text{AHP}_{12} + 6 \text{AHP}_{16} + 3 \{2 \text{AHP}_{36} + \text{AHP}_{38}\} \\ &= -11.73 \text{ eV}. \quad (25) \end{aligned}$$

Note, incidentally, the small positive (repulsive) AHP's between carbon and hydrogen atoms attached to the neighboring carbon atom and two hydrogen atoms attached to the same or different carbon atoms — the exception being the tiny attractive *trans*-H-H interaction.

We proceed next to extended, translationally periodic systems.

VII. DEFINING THE TOTAL ELECTRONIC ENERGY FOR AN EXTENDED SYSTEM

Consider the i th eigenfunction resulting from solution of the generalized eigenvalue problem (26) for a general point, \mathbf{k} in reciprocal space,

$$\mathbf{H}(\mathbf{k}) \mathbf{C} = \mathbf{E} \mathbf{S}(\mathbf{k}) \mathbf{C}, \quad (26)$$

where $\mathbf{E} \equiv \mathbf{E}(\mathbf{k})$ and $\mathbf{C} \equiv \mathbf{C}(\mathbf{k})$ are the matrices containing the eigenvalues and eigenvectors respectively. $\mathbf{H}(\mathbf{k})$ and $\mathbf{S}(\mathbf{k})$ denote, respectively, the Hamiltonian and overlap matrices. The i th eigenvalue is given by

$$\mathbf{E}_i(\mathbf{k}) = \frac{\langle \psi_i(\mathbf{k}) | \hat{\mathbf{H}} | \psi_i(\mathbf{k}) \rangle}{\langle \psi_i(\mathbf{k}) | \psi_i(\mathbf{k}) \rangle}. \quad (27)$$

The crystal orbitals, $\{\psi_i(\mathbf{k})\}$ are generated as a sum over a Bloch basis $\{\phi_\mu(\mathbf{k})\}$ [Eq. (28)]. The Bloch sum (29) for the μ th valence (or unit cell) basis function, U_μ , is defined as a sum over all lattice vectors, \mathbf{R} with reference to an arbitrary origin or ‘‘home cell’’ within the lattice,

$$\psi_i(\mathbf{r}, \mathbf{k}) = \sum_\mu c_{\mu i} \phi_\mu, \quad (28)$$

$$\phi_\mu(\mathbf{r}, \mathbf{k}) = \sum_{\mathbf{R}} U_\mu(\mathbf{r} - \mathbf{R}) e^{i\mathbf{k} \cdot \mathbf{R}}. \quad (29)$$

On substituting Eqs. (28) and (29) in Eq. (27) the expression for the i th eigenvalue at a general point, \mathbf{k} in reciprocal space becomes

$$\mathbf{E}_i(\mathbf{k}) = \frac{1}{\langle \psi_i(\mathbf{k}) | \psi_i(\mathbf{k}) \rangle} \sum_\mu \sum_\nu \sum_{\mathbf{R}_1} \sum_{\mathbf{R}_2} c_{\mu i}^* c_{\nu i} \times e^{i\mathbf{k} \cdot (\mathbf{R}_2 - \mathbf{R}_1)} \langle U_\mu(\mathbf{R}_1) | \hat{\mathbf{H}} | U_\nu(\mathbf{R}_2) \rangle. \quad (30)$$

The notation $U_\mu(\mathbf{R}) \equiv U_\mu(\mathbf{r} - \mathbf{R})$ is introduced to simplify the form of Eq. (30) and all subsequent expressions. The total electronic energy for an extended system (for a discrete sampling in reciprocal space) is given by Eq. (31),

$$\mathbf{E}_{\text{tot}} = \sum_{\mathbf{k} \in \mathcal{K}} \sum_i \Omega_{\mathbf{k}} n_i(\mathbf{k}) \mathbf{E}_i(\mathbf{k}). \quad (31)$$

The total electronic energy (31) is defined as a summation over crystal orbitals (CO’s) — occupancy $n_i(\mathbf{k})$, for each reciprocal space point \mathbf{k} belonging to the discrete set \mathcal{K} — each with an associated weighting, $\Omega_{\mathbf{k}}$. By analogy with the molecular case described previously the immediate goal is to express the total electronic energy (31) as a sum over Hamiltonian matrix elements [see Eq. (7)]. Substituting Eq. (30) in Eq. (31) gives, on performing the change of variable $\mathbf{R} = \mathbf{R}_1$ and $\mathbf{R}' = (\mathbf{R}_2 - \mathbf{R}_1)$,

$$\mathbf{E}_{\text{tot}} = \sum_{\mathbf{k} \in \mathcal{K}} \sum_i \frac{\Omega_{\mathbf{k}} n_i(\mathbf{k})}{\langle \psi_i(\mathbf{k}) | \psi_i(\mathbf{k}) \rangle} \left\{ \sum_{\mathbf{R}} e^{i\mathbf{k} \cdot \mathbf{R}} \sum_{\mathbf{R}'} \sum_\mu \sum_\nu c_{\mu i}^* c_{\nu i} \times e^{i\mathbf{k} \cdot (\mathbf{R}' - \mathbf{R})} \mathbf{H}_{\mu\nu}(\mathbf{R}' - \mathbf{R}) \right\}, \quad (32)$$

where we have defined $\mathbf{H}_{\mu\nu}(\mathbf{R}' - \mathbf{R}) = \langle U_\mu(\mathbf{R}) | \hat{\mathbf{H}} | U_\nu(\mathbf{R} + \mathbf{R}') \rangle$. The Hamiltonian matrix element, $\mathbf{H}_{\mu\nu}(\mathbf{R}' - \mathbf{R})$ describes the interaction between valence basis functions U_μ and U_ν in unit cells defined by the lattice vectors \mathbf{R} and $\mathbf{R} + \mathbf{R}'$, respectively, and is a function of the vector $(\mathbf{R}' - \mathbf{R})$. Thus, on defining the change of variable $\mathbf{R}'' = (\mathbf{R}' - \mathbf{R})$ Eq. (32) becomes

$$\mathbf{E}_{\text{tot}} = \sum_{\mathbf{k} \in \mathcal{K}} \sum_i \frac{\Omega_{\mathbf{k}} n_i(\mathbf{k})}{\langle \psi_i(\mathbf{k}) | \psi_i(\mathbf{k}) \rangle} \left\{ \sum_{\mathbf{R}} e^{i\mathbf{k} \cdot \mathbf{R}} \sum_{\mathbf{R}''} \sum_\mu \sum_\nu c_{\mu i}^* c_{\nu i} \times e^{i\mathbf{k} \cdot \mathbf{R}''} \mathbf{H}_{\mu\nu}(\mathbf{R}'') \right\}, \quad (33)$$

where $\mathbf{H}_{\mu\nu}(\mathbf{R}'') = \langle U_\mu(\mathbf{0}) | \hat{\mathbf{H}} | U_\nu(\mathbf{R}'') \rangle$ denotes the interaction between the valence basis function $U_\mu(\mathbf{0})$ in the ‘‘home cell’’ and $U_\nu(\mathbf{R}'')$ in the unit cell defined by the lattice vector \mathbf{R}'' with respect to the home cell.

Let us now consider the corresponding expression for the total electronic energy when dealing with normalized crystal orbitals. By analogy with the treatment of the Hamiltonian matrix element, $\langle \psi_i(\mathbf{k}) | \hat{\mathbf{H}} | \psi_i(\mathbf{k}) \rangle$ presented above, the overlap matrix element, $\langle \psi_i(\mathbf{k}) | \psi_i(\mathbf{k}) \rangle$ can be written as

$$\langle \psi_i(\mathbf{k}) | \psi_i(\mathbf{k}) \rangle = \sum_{\mathbf{R}} e^{i\mathbf{k} \cdot \mathbf{R}} \sum_{\mathbf{R}''} \sum_\mu \sum_\nu c_{\mu i}^* c_{\nu i} e^{i\mathbf{k} \cdot \mathbf{R}''} \mathbf{S}_{\mu\nu}(\mathbf{R}''), \quad (34)$$

on defining $\mathbf{S}_{\mu\nu}(\mathbf{R}'') = \langle U_\mu(\mathbf{0}) | U_\nu(\mathbf{R}'') \rangle$.

Thus, on substituting Eq. (34) into Eq. (33) the normalization condition becomes

$$\sum_{\mathbf{R}''} \sum_\mu \sum_\nu c_{\mu i}^* c_{\nu i} e^{i\mathbf{k} \cdot \mathbf{R}''} \mathbf{S}_{\mu\nu}(\mathbf{R}'') = 1, \quad (35)$$

for each reciprocal space point, $\mathbf{k} \in \mathcal{K}$.

From this point on we shall consider a normalized set of crystal orbitals, for which the expression for the total electronic energy, Eq. (33) is written

$$\begin{aligned} \mathbf{E}_{\text{tot}} &= \sum_{\mathbf{k} \in \mathcal{K}} \sum_i \Omega_{\mathbf{k}} n_i(\mathbf{k}) \sum_{\mathbf{R}''} \sum_\mu \sum_\nu c_{\mu i}^* c_{\nu i} e^{i\mathbf{k} \cdot \mathbf{R}''} \mathbf{H}_{\mu\nu}(\mathbf{R}'') \\ &= \sum_{\mathbf{k} \in \mathcal{K}} \sum_i \Omega_{\mathbf{k}} n_i(\mathbf{k}) \left\{ \sum_\mu \sum_\nu c_{\mu i}^* c_{\nu i} \mathbf{H}_{\mu\nu}(\mathbf{0}) \right. \\ &\quad \left. + \sum_{\mathbf{R}'' \neq \mathbf{0}} \sum_\mu \sum_\nu c_{\mu i}^* c_{\nu i} e^{i\mathbf{k} \cdot \mathbf{R}''} \mathbf{H}_{\mu\nu}(\mathbf{R}'') \right\}. \end{aligned} \quad (36)$$

In order to simplify an analysis of the total electronic energy distribution for the lattice it is desirable to reduce the number of intercell ($\mathbf{R}'' \neq \mathbf{0}$) terms in Eq. (36). The lattice vectors \mathbf{R}'' are given in Eq. (37) in terms of the primitive lattice translations \mathbf{a} , \mathbf{b} , and \mathbf{c} for integers α , β , and γ ,

$$\mathbf{R}'' = \alpha \mathbf{a} + \beta \mathbf{b} + \gamma \mathbf{c}. \quad (37)$$

The summation over \mathbf{R}'' can be partitioned as follows:

$$\sum_{\mathbf{R}'' \neq \mathbf{0}} = \sum_{\mathbf{R}'' \in \mathbf{R}^+} + \sum_{\mathbf{R}'' \in \mathbf{R}^-}, \quad (38)$$

on defining the sets of lattice vectors \mathbf{R}^+ and \mathbf{R}^- by Eqs. (39) and (40), respectively,

$$\begin{aligned} \mathbf{R}^+ &= \{\alpha > 0, \beta = 0, \gamma = 0\} \\ &\cup \{\text{integer } \alpha, \beta > 0, \gamma = 0\} \\ &\cup \{\text{integer } \alpha \text{ and } \beta, \gamma > 0\}, \end{aligned} \quad (39)$$

$$\begin{aligned} \mathbf{R}^- &= \{\alpha < 0, \beta = 0, \gamma = 0\} \\ &\cup \{\text{integer } \alpha, \beta < 0, \gamma = 0\} \\ &\cup \{\text{integer } \alpha \text{ and } \beta, \gamma < 0\}. \end{aligned} \quad (40)$$

The sets of unit cells defined by summing over the sets of lattice vectors \mathbf{R}^+ and \mathbf{R}^- are illustrated in Fig. 2 for a cubic crystal system.

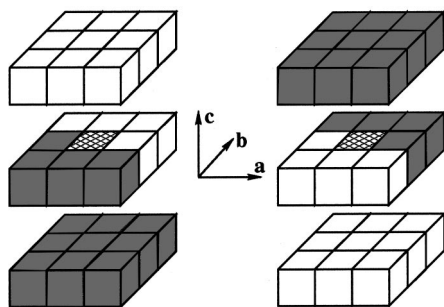


FIG. 2. The unit cells defined by (a) the \mathbf{R}^- set of lattice vectors (shaded) and (b) the \mathbf{R}^+ set of lattice vectors (shaded), with respect to the lattice vectors $(\mathbf{a}, \mathbf{b}, \mathbf{c})$ for a cubic lattice relative to the "home cell" (hatched).

For a set of valence basis functions, $\{U_i\}$ the summation over the set of lattice vectors \mathbf{R}^- can be rewritten as a sum over the set \mathbf{R}^+ on utilizing Eq. (41) for all valence (unit cell) basis functions μ and ν ,

$$\langle U_\mu(\mathbf{0}) | \hat{\mathbf{H}} | U_\nu(-\mathbf{R}'') \rangle \equiv \langle U_\nu(\mathbf{0}) | \hat{\mathbf{H}} | U_\mu(\mathbf{R}'') \rangle^*. \quad (41)$$

Thus the total electronic energy (36) can be written as a limited summation over lattice vectors $\mathbf{R}'' \in \mathbf{R}^+$ in accord with Eq. (42),

$$\begin{aligned} E_{\text{tot}} = & \sum_{\mathbf{k} \in \mathcal{K}} \sum_{\text{CO}'s} \Omega_{\mathbf{k}} n_i(\mathbf{k}) \left\{ \sum_{\mu} \sum_{\nu} c_{\mu i}^* c_{\nu i} \mathbf{H}_{\mu\nu}(\mathbf{0}) \right. \\ & + \sum_{\mathbf{R}'' \in \mathbf{R}^+} \sum_{\mu} \sum_{\nu} \{ c_{\mu i}^* c_{\nu i} e^{i\mathbf{k} \cdot \mathbf{R}''} \mathbf{H}_{\mu\nu}(\mathbf{R}'') \\ & \left. + c_{\mu i} c_{\nu i}^* e^{-i\mathbf{k} \cdot \mathbf{R}''} \mathbf{H}_{\mu\nu}^*(\mathbf{R}'') \right\}. \quad (42) \end{aligned}$$

The energy partitioning (42) is applicable to all methods utilizing an atom localized basis set and a one-electron formalism. It is also worth noting that on reducing the double summation over lattice vectors \mathbf{R}_1 and \mathbf{R}_2 to a sum over $\mathbf{R}'' \in \mathbf{R}^+$, the total electronic energy can be written as a sum over Hamiltonian matrix elements which involve one or more valence basis functions in the unit cell hereafter referred to as the "home cell," defined by $\mathbf{R}'' = \mathbf{0}$.

VIII. CRYSTAL ORBITAL HAMILTON POPULATIONS (COHP'S)

In this section the total electronic energy (42) will be used to define the "Crystal Orbital Hamilton Population (COHP)," previously introduced by Dronskowski and Blöchl.¹ An intra/intercell energy partitioning follows immediately from Eq. (42). The intracell term from Eq. (42) can be partitioned into on- and off-site terms according to Eq. (43),

$$\begin{aligned} & \sum_{\mu} \sum_{\nu} c_{\mu i}^* c_{\nu i} \langle U_\mu(\mathbf{0}) | \hat{\mathbf{H}} | U_\nu(\mathbf{0}) \rangle \\ & = \sum_{\mu} |c_{\mu i}|^2 \mathbf{H}_{\mu\mu}(\mathbf{0}) + \frac{1}{2} \sum_{\mu} \sum_{\nu \neq \mu} \{ c_{\mu i}^* c_{\nu i} \mathbf{H}_{\mu\nu}(\mathbf{0}) \\ & \quad + c_{\mu i} c_{\nu i}^* \mathbf{H}_{\nu\mu}(\mathbf{0}) \}, \quad (43) \end{aligned}$$

By analogy with the molecular case [Eqs. (5) and (6)] on- and off-site COHP's within the home unit cell are defined by Eqs. (44) and (45), respectively,

$$\text{COHP}_{\mu\mu}(\mathbf{0}) = \sum_{\mathbf{k} \in \mathcal{K}} \Omega_{\mathbf{k}} \sum_{\text{CO}'s} n_i(\mathbf{k}) |c_{\mu i}|^2 \mathbf{H}_{\mu\mu}(\mathbf{0}), \quad (44)$$

$$\begin{aligned} \text{COHP}_{\mu\nu}(\mathbf{0}) = & \sum_{\mathbf{k} \in \mathcal{K}} \Omega_{\mathbf{k}} \sum_{\text{CO}'s} n_i(\mathbf{k}) \{ c_{\mu i}^* c_{\nu i} \mathbf{H}_{\mu\nu}(\mathbf{0}) \\ & + c_{\mu i} c_{\nu i}^* \mathbf{H}_{\nu\mu}(\mathbf{0}) \}. \quad (45) \end{aligned}$$

On defining the intercell COHP between basis functions μ in the home cell and ν in the cell defined by lattice vector \mathbf{R} (with respect to the home unit cell) by Eq. (46), the total electronic energy (42) can be expressed as a sum over on-site intracell, off-site intracell, and intercell COHP's as defined by Eqs. (44), (45) and (46), respectively,

$$\begin{aligned} \text{COHP}_{\mu\nu}(\mathbf{R}) = & \sum_{\mathbf{k} \in \mathcal{K}} \Omega_{\mathbf{k}} \sum_{\text{CO}'s} n_i(\mathbf{k}) \{ c_{\mu i}^* c_{\nu i} e^{i\mathbf{k} \cdot \mathbf{R}} \mathbf{H}_{\mu\nu}(\mathbf{R}) \\ & + c_{\mu i} c_{\nu i}^* e^{-i\mathbf{k} \cdot \mathbf{R}} \mathbf{H}_{\mu\nu}^*(\mathbf{R}) \}. \quad (46) \end{aligned}$$

Thus the total electronic energy can be partitioned according to Eq. (47):

$$\begin{aligned} E_{\text{tot}} = & \sum_{\mu} \text{COHP}_{\mu\mu}(\mathbf{0}) + \frac{1}{2} \sum_{\mu} \sum_{\nu \neq \mu} \text{COHP}_{\mu\nu}(\mathbf{0}) \\ & + \sum_{\mathbf{R} \in \mathbf{R}^+} \sum_{\mu} \sum_{\nu} \text{COHP}_{\mu\nu}(\mathbf{R}). \quad (47) \end{aligned}$$

The COHP formulation (47) differs from that of Dronskowski and Blöchl¹ only by treating intercell COHP terms (46) explicitly. The intercell and intracell terms in (47) are combined in the treatment of Dronskowski and Blöchl, resulting in a loss of spatial information beyond the bounds of the home unit cell. The strength of the current COHP formulation is the ability to localize changes in electronic structure in real space resulting from a structural change within the unit cell.

IX. A HAMILTON POPULATION STUDY OF THE Pt-Pt INTERACTION IN $[\text{PtH}_4]^{2-}$

The mechanics of Hamilton population analysis for extended materials may be illustrated by application to a simple one-dimensional hypothetical polymer. Consider the chain constructed by stacking square planar $[\text{PtH}_4]^{2-}$ monomers in an eclipsed conformation at a separation of 3 Å as illustrated in Fig. 3. This system has been studied earlier.^{2,22}

For the sake of simplicity we concentrate on σ interactions between platinum atoms. These are determined by three orbitals on each platinum center, the s , p_z , and d_{z^2} valence orbitals – the chain direction being defined as the z direction as shown in Fig. 3. Following Eq. (47) the σ component of the Pt-Pt interaction can be written

$$E_{\sigma(\text{Pt-Pt})} = \sum_{\mathbf{R} \in \mathbf{R}^+} \sum_{\mu \in \Sigma} \sum_{\nu \in \Sigma} \text{COHP}_{\mu\nu}(\mathbf{R}), \quad (48)$$

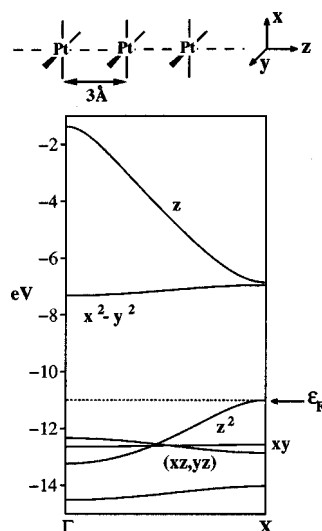


FIG. 3. Band structure for $\frac{1}{3}[\text{PtH}_4]^{2-}$. Three of the low-lying Pt–H bonding bands and the Pt-centered s , p_x , and p_y Pt–H antibonding bands have been omitted.

for the valence orbital set $\Sigma = \{s, p_z, d_{z^2}\}$.

The relatively large Pt–Pt separation of 3 Å effectively reduces the sum of interactions over lattice vectors $\mathbf{R} \in \mathbf{R}^+$ to the interaction between Pt orbitals in nearest neighbor cells. Thus Eq. (48) can be written

$$\mathbf{E}_{\sigma(\text{Pt-Pt})} = \sum_{\mu \in \Sigma} \sum_{\nu \in \Sigma} \text{COHP}_{\mu\nu}(\mathbf{1}). \quad (49)$$

The results of the Hamilton population analysis are summarized in Table III along with the results of an analogous overlap population analysis.

As can be seen on examining Table III, Pt–Pt σ interactions are composed almost exclusively of p_z – d_{z^2} and, to a lesser extent, s – p_z valence orbital interactions between neighboring Pt centers. Despite a larger physical overlap — the overlap between s and p_z valence orbitals being approximately twice that of p_z and d_{z^2} orbitals on adjacent Pt centers — the Pt–Pt s – p_z overlap population is calculated to be $\sim 50\%$ of the p_z – d_{z^2} overlap population. This is due to a greater degree of mixing between the Pt p_z and d_{z^2} bands, the relatively high energy Pt s band (band center ~ 9 eV) relegating sp interactions between neighboring Pt atoms to a minor role in Pt–Pt σ bonding.

While in general the Hamilton population analysis parallels the overlap population analysis in this system, there is a difference. Note the approximately 2:1 ratio of p_z – d_{z^2} to

s – p_z overlap populations in contrast to the corresponding Hamilton population ratio of approximately 3:1. Both approaches give a small repulsive d_{z^2} – d_{z^2} interaction, perhaps smaller than one might have anticipated. Clearly the more diffuse Pt s and p orbitals can participate to a greater extent in Pt–Pt interaction.

We now continue our development of the formalism for extended systems.

X. COHP'S: AN EXTENDED HÜCKEL APPROACH

The familiar Wolfsberg–Helmholtz approximation to $\mathbf{H}_{\mu\nu}$ (Ref. 18) can be used to generate the following on- and off-site COHP's, based on Eqs. (44), (45), and (46) respectively,

$$\text{COHP}_{\mu\mu}(\mathbf{0}) = \sum_{\mathbf{k} \in \mathcal{K}} \Omega_{\mathbf{k}} \sum_{\text{CO}'_s} n_i(\mathbf{k}) |c_{\mu i}|^2 \mathbf{H}_{\mu\mu}, \quad (50)$$

$$\begin{aligned} \text{COHP}_{\mu\nu}(\mathbf{R}) = & \sum_{\mathbf{k} \in \mathcal{K}} \Omega_{\mathbf{k}} \sum_{\text{CO}'_s} n_i(\mathbf{k}) \{c_{\mu i}^* c_{\nu i} \mathbf{e}^{i\mathbf{k} \cdot \mathbf{R}} \\ & + c_{\mu i} c_{\nu i}^* \mathbf{e}^{-i\mathbf{k} \cdot \mathbf{R}}\} \kappa_{\mu\nu} \mathbf{S}_{\mu\nu}(\mathbf{R}), \end{aligned} \quad (51)$$

where $\mathbf{H}_{\mu\mu}$ is the diagonal matrix element of the molecular Hamiltonian matrix corresponding to the μ th valence basis function, $\mathbf{S}_{\mu\nu}(\mathbf{R}) \equiv \langle \mathbf{U}_{\mu}(\mathbf{0}) | \mathbf{U}_{\nu}(\mathbf{R}) \rangle$ and $\kappa_{\mu\nu}$ is defined by Eq. (8). COOP analogs, intimately related to the COHP's (50) and (51) can be formulated within an extended Hückel framework, and are given by Eqs. (52) and (53), respectively,

$$\text{COOP}_{\mu\mu}(\mathbf{0}) = \sum_{\mathbf{k} \in \mathcal{K}} \Omega_{\mathbf{k}} \sum_{\text{CO}'_s} n_i(\mathbf{k}) |c_{\mu i}|^2, \quad (52)$$

$$\begin{aligned} \text{COOP}_{\mu\nu}(\mathbf{R}) = & \sum_{\mathbf{k} \in \mathcal{K}} \Omega_{\mathbf{k}} \sum_{\text{CO}'_s} n_i(\mathbf{k}) \{c_{\mu i}^* c_{\nu i} \mathbf{e}^{i\mathbf{k} \cdot \mathbf{R}} \\ & + c_{\mu i} c_{\nu i}^* \mathbf{e}^{-i\mathbf{k} \cdot \mathbf{R}}\} \mathbf{S}_{\mu\nu}(\mathbf{R}). \end{aligned} \quad (53)$$

XI. SCHEMES FOR TOTAL ELECTRONIC ENERGY PARTITIONING IN EXTENDED SYSTEMS

In this section atom and fragment based energy partitioning schemes for extended systems (analogous to those of Sec. V for molecular systems) are developed.

On defining $\mathcal{A}^{(i)}$ as the set of valence basis functions centered on the i th atom within the home unit cell, the crystal orbital partitioning (47) can be recast in the atom-based form

$$\begin{aligned} \mathbf{E}_{\text{tot}} = & \sum_{\text{ATOMS}} \text{CAHP}_i(\mathbf{0}) + \frac{1}{2} \sum_{\text{ATOMS}} \sum_{\substack{\text{ATOMS} \\ j \neq i}} \text{CAHP}_{ij}(\mathbf{0}) \\ & + \sum_{\mathbf{R} \in \mathbf{R}^+} \sum_{\text{ATOMS}} \sum_{\text{ATOMS}} \text{CAHP}_{ij}(\mathbf{R}). \end{aligned} \quad (54)$$

In the above expression on- and off-site Crystal Atom Hamilton Populations (CAHP's), CAHP_i , and CAHP_{ij} , respectively, are defined for an orthogonal valence basis on each atomic center by

TABLE III. Comparative overlap and Hamilton population analyses of Pt–Pt σ bonding in $\frac{1}{3}[\text{PtH}_4]^{2-}$.

σ component	Pt–Pt OP	Pt–Pt HP/eV
s – s	–0.001	0.01
s – p	0.019	–0.25
s – d	0.001	–0.01
p – p	0.001	–0.01
p – d	0.041	–0.70
d – d	–0.003	0.07

$$\text{CAHP}_i(\mathbf{0}) = \sum_{\mu \in \mathcal{A}^{(i)}} \text{COHP}_{\mu\mu}(\mathbf{0}), \quad (55)$$

and

$$\text{CAHP}_{ij}(\mathbf{R}) = \sum_{\mu \in \mathcal{A}^{(i)}} \sum_{\nu \in \mathcal{A}^{(j)}} \text{COHP}_{\mu\nu}(\mathbf{R}). \quad (56)$$

Again by analogy with the molecular case (see Sec. V) crystal fragments can be defined — a crystal fragment being a subset of all atoms in the home unit cell. The total electronic energy for an extended system (47) can be expressed as a sum over intra- and intercrystal fragment Hamiltonian populations, as defined by Eqs. (58) and (59), respectively. On defining the set $\mathcal{B}^{(m)}$ containing the atoms belonging to the m th fragment, the total electronic energy for an extended material is written,

$$\begin{aligned} \mathbf{E}_{\text{tot}} = & \sum_m \text{CFHP}_m(\mathbf{0}) + \frac{1}{2} \sum_m \sum_{n \neq m} \text{CFHP}_{mn}(\mathbf{0}) \\ & + \sum_{\mathbf{R} \in \mathbf{R}^+} \sum_m \sum_n \text{CFHP}_{mn}(\mathbf{R}). \end{aligned} \quad (57)$$

$$\begin{aligned} \text{CFHP}_m(\mathbf{0}) = & \sum_{i \in \mathcal{B}^{(m)}} \text{CAHP}_i(\mathbf{0}) \\ & + \frac{1}{2} \sum_{i \in \mathcal{B}^{(m)}} \sum_{\substack{j \in \mathcal{B}^{(m)} \\ j \neq i}} \text{CAHP}_{ij}(\mathbf{0}), \end{aligned} \quad (58)$$

$$\text{CFHP}_{mn}(\mathbf{R}) = \sum_{i \in \mathcal{B}^{(m)}} \sum_{j \in \mathcal{B}^{(n)}} \text{CAHP}_{ij}(\mathbf{R}). \quad (59)$$

The crystal fragment energy partitioning will be employed in the final section of this paper to analyze surface–adsorbate interactions in the CO/Ni(100) chemisorption system. The surface layer and underlying “bulk” Ni layers of the Ni slab model are there treated as separate crystal fragments for the purpose of the analysis. Such a fragment-based analysis is frequently followed by a more “localized” analysis, for example an orbital-by-orbital study. When electing to perform an orbital-based analysis, a fragment crystal orbital (FCO) basis is generally preferable over an atom-localized valence orbital basis, in order to maintain the integrity of the fragment by fragment interaction scheme developed previously. Surface–adsorbate interactions, such as those in the CO/Ni(100) system studied in this paper, are particularly amenable to FCO analysis.

XII. TOTAL ELECTRONIC ENERGY PARTITIONING IN A FRAGMENT ORBITAL BASIS

The discussions of the preceding sections will now be reformulated in a language of fragment molecular orbitals (FMO's) and fragment crystal orbitals (FCO's) for molecular and extended systems, respectively.

For a molecular system a fragment is defined simply as a subset of all atoms in the molecule, FMO's for the m th fragment $\{\chi_\nu^{(m)}, \nu \in \mathcal{C}^{(m)}\}$ being constructed as a linear combination of the valence basis functions associated with the atoms belonging to the m th fragment, $\{\phi_\nu^{(m)}, \nu \in \mathcal{D}^{(m)}\}$, as given by

$$\chi_\nu^{(m)} = \sum_{\alpha \in \mathcal{D}^{(m)}} d_{\alpha\nu}^{(m)} \phi_\alpha^{(m)}. \quad (60)$$

By analogy with Eq. (1), the i th wave function for the molecular system in the FMO basis is written

$$\psi_i^{\text{FMO}} = \sum_j \sum_{\mu \in \mathcal{C}^{(j)}} c_{\mu i}^{(j)} \chi_\mu^{(j)},$$

where

$$\langle \psi_i^{\text{FMO}} | \psi_i^{\text{FMO}} \rangle = 1 \text{ for all } i. \quad (61)$$

The total electronic energy for a molecular system (4) becomes

$$\begin{aligned} \mathbf{E}_{\text{tot}} = & \sum_i \sum_{\text{M.O.'s}} n_i \left\{ \sum_j \sum_{\mu \in \mathcal{C}^{(j)}} |c_{\mu i}^{(j)}|^2 \mathbf{H}_{\mu\mu}^{jj} \right. \\ & \left. + \sum_j \sum_{\substack{\text{FRAGS} \\ l \neq j}} \sum_{\mu \in \mathcal{C}^{(j)}} \sum_{\nu \in \mathcal{C}^{(l)}} [c_{\mu i}^{(j)}]^* c_{\nu i}^{(l)} \mathbf{H}_{\mu\nu}^{jl} \right\}, \end{aligned} \quad (62)$$

on defining $\mathbf{H}_{\mu\nu}^{jl} \equiv \langle \chi_\mu^{(j)} | \hat{\mathbf{H}} | \chi_\nu^{(l)} \rangle$ and noting that $\mathbf{H}_{\mu\nu}^{jj} = \delta_{\mu\nu} \mathbf{H}_{\mu\mu}^{jj}$ for all fragments j such that $(\mu, \nu) \in \mathcal{C}^{(j)}$.

Equation (62) is a total molecular electronic energy partitioning in a FMO basis and can be expressed as a sum over intra- and interfragment energy contributions, as defined by Eqs. (64) and (65), respectively,

$$\mathbf{E}_{\text{tot}} = \sum_j \text{FHP}_j^{\text{FMO}} + \frac{1}{2} \sum_j \sum_{\substack{\text{FRAGS} \\ l \neq j}} \text{FHP}_{jl}^{\text{FMO}}, \quad (63)$$

$$\text{FHP}_j^{\text{FMO}} = \sum_i \sum_{\mu \in \mathcal{C}^{(j)}} n_i |c_{\mu i}^{(j)}|^2 \mathbf{H}_{\mu\mu}^{jj}, \quad (64)$$

$$\begin{aligned} \text{FHP}_{jl}^{\text{FMO}} = & \sum_i \sum_{\mu \in \mathcal{C}^{(j)}} \sum_{\nu \in \mathcal{C}^{(l)}} n_i \{ [c_{\mu i}^{(j)}]^* c_{\nu i}^{(l)} \mathbf{H}_{\mu\nu}^{jl} \\ & + c_{\mu i}^{(j)} [c_{\nu i}^{(l)}]^* \mathbf{H}_{\nu\mu}^{jl} \}. \end{aligned} \quad (65)$$

The extended system analog of Eq. (63) is derived from a crystal fragment orbital (CFO) basis — $\chi_\mu^{(j)}$ being defined as the μ th CFO belonging to the j th fragment. The i th crystal orbital is written as a sum over CFO's according to

$$\psi_i^{\text{FCO}} = \sum_j \sum_{\mu \in \mathcal{C}^{(j)}} c_{\mu i}^{(j)} \chi_\mu^{(j)}, \quad (66)$$

$\mathcal{C}^{(j)}$ being defined as the set of CFO's belonging to the j th fragment. The CFO's belonging to the j th fragment $\{\chi_\mu^{(j)}, \mu \in \mathcal{C}^{(j)}\}$ are constructed from the valence basis associated with the j th fragment, $\mathcal{D}^{(j)}$ and are given by

$$\begin{aligned} \chi_\mu^{(j)} = & \sum_{\alpha \in \mathcal{D}^{(j)}} d_{\alpha\mu}^{(j)} \phi_\alpha^{(j)} \\ = & \sum_{\mathbf{R}} \left\{ \sum_{\alpha \in \mathcal{D}^{(j)}} d_{\alpha\mu}^{(j)} U_\alpha^{(j)}(\mathbf{r} - \mathbf{R}) \right\} \mathbf{e}^{i\mathbf{k} \cdot \mathbf{R}}, \end{aligned} \quad (67)$$

for a Bloch valence basis, $\{\phi_\alpha^{(j)}(\mathbf{r}, \mathbf{k})\}$ defined by Eq. (29).

The total electronic energy for an extended system (47) can be partitioned into a sum over on- and off-fragment crystal fragment Hamilton populations (CFHP's). The on-fragment energy contribution for the j th fragment in the home unit cell is defined by Eq. (68) and is analogous to on-site COHP's (44) defined with respect to an atom localized valence basis set. Off-fragment energy contributions between fragments j and l in the home cell, $\text{CFHP}_{jl}^{\text{FMO}}(\mathbf{0})$ and fragments j and l in unit cells separated by a lattice vector \mathbf{R} , $\text{CFHP}_{jl}^{\text{FMO}}(\mathbf{R})$ are defined by Eq. (69). Equation (69) is analogous to the off-site COHP defined by Eq. (46),

$$\text{CFHP}_j^{\text{FMO}}(\mathbf{0}) = \sum_{k \in \mathcal{K}} \sum_{i \in \text{CO's}} \Omega_k n_i(\mathbf{k}) \left\{ \sum_{\mu \in \mathcal{C}^{(j)}} \sum_{\alpha \in \mathcal{D}^{(j)}} \sum_{\beta \in \mathcal{D}^{(j)}} \times d_{\alpha\mu}^{(j)} d_{\beta\mu}^{(j)} |c_{\mu i}^{(j)}|^2 \mathbf{H}_{\alpha\beta}^{jj}(\mathbf{0}) \right\}, \quad (68)$$

$$\text{CFHP}_{jl}^{\text{FMO}}(\mathbf{R}) = \sum_{k \in \mathcal{K}} \sum_{i \in \text{CO's}} \Omega_k n_i(\mathbf{k}) \left\{ \sum_{\mu \in \mathcal{C}^{(j)}} \sum_{\nu \in \mathcal{C}^{(l)}} \sum_{\alpha \in \mathcal{D}^{(j)}} \times \sum_{\beta \in \mathcal{D}^{(l)}} d_{\alpha\mu}^{(j)} d_{\beta\nu}^{(l)} \cdot \{ [c_{\mu i}^{(j)}]^* c_{\nu i}^{(l)} e^{i\mathbf{k} \cdot \mathbf{R}} \mathbf{H}_{\alpha\beta}^{jl}(\mathbf{R}) + c_{\mu i}^{(j)} [c_{\nu i}^{(l)}]^* e^{-i\mathbf{k} \cdot \mathbf{R}} \mathbf{H}_{\alpha\beta}^{jl*}(\mathbf{R}) \} \right\}, \quad (69)$$

where $\mathbf{H}_{\alpha\beta}^{jl}(\mathbf{R}) \equiv \langle U_{\alpha}^{(j)}(\mathbf{0}) | \hat{\mathbf{H}} | U_{\beta}^{(l)}(\mathbf{R}) \rangle$ for $\alpha \in \mathcal{D}^{(j)}, \beta \in \mathcal{D}^{(l)}$.

Equation (70) effects a CFHP total electronic energy partitioning for an extended system,

$$\mathbf{E}_{\text{tot}} = \sum_{j \in \text{FRAGS}} \text{CFHP}_j^{\text{FMO}}(\mathbf{0}) + \frac{1}{2} \sum_{j \in \text{FRAGS}} \sum_{l \neq j \in \text{FRAGS}} \text{CFHP}_{jl}^{\text{FMO}}(\mathbf{0}) + \sum_{\mathbf{R} \in \mathbf{R}^+} \sum_{j \in \text{FRAGS}} \sum_{l \in \text{FRAGS}} \text{CFHP}_{jl}^{\text{FMO}}(\mathbf{R}). \quad (70)$$

It is high time for an example.

XIII. A HAMILTON POPULATION STUDY OF BONDING IN C(2×2)-CO/Ni(100)

We have used overlap populations for a long time, and they have proven extremely useful in helping us reach an understanding of bonding across the Periodic Table. Hamilton populations and energy partitioning are new to us. It will take some time to develop an idea of how useful this promising tool is. We will see the range and validity of the applications in future studies; here we begin by reanalyzing a previously studied system.

Surface-adsorbate interactions have been extensively studied from both an experimental and theoretical standpoint in recent decades, yet many aspects of the subject remain unclear. The CO/Ni(100) system is perhaps the most extensively studied metal-CO chemisorption system.⁵⁻¹⁴ Carbon monoxide — a σ donor and π acceptor — is a prototypical adsorbate for studies of surface-adsorbate interaction. Metal surface-CO interactions are traditionally described by the 5σ to metal forward donation, and metal to 2π backdonation model proposed by Blyholder²³ — an extension to metal

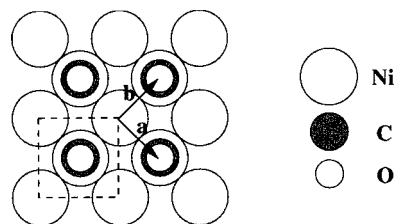


FIG. 4. A centered (2×2) array of CO chemisorbed on the Ni(100) surface as viewed along the surface normal (c). The dashed lines indicate the boundaries of the supercell used to model the $c(2 \times 2)$ -CO/Ni(100) system.

surfaces of the Dewar-Chatto-Duncanson model of metal-ligand organometallic bonding. Within that model, the bonding role, if any, of low-lying CO orbitals, specifically the 4σ orbital,²⁴ is not clear. Recent x-ray emission studies of CO chemisorption on the Ni(100) surface by Nilsson *et al.*⁵ suggest a bonding role for the CO 4σ orbital, in agreement with the CO 4σ bonding role proposed earlier by our group for CO chemisorption on the M(111) (M=Ni, Pd, Pt) surfaces²⁵ and the model proposed by Hu *et al.* for CO chemisorption on the Pd(110) surface.²⁶ These studies are in marked contrast to the recent theoretical study of CO chemisorption on the Pt(111) surface by Aizawa and Tsuneyuki²⁷ which favors a simpler Blyholder frontier orbital model of the CO-surface interaction. The Hamilton population analyses presented in this section address specifically the relative importance of CO 4σ , 5σ , and $2\pi^*$ orbital interactions with the Ni(100) surface.

Another aspect of the surface-CO interaction which remains relatively unclear is the relative importance of metal s , p , and d bands in binding CO to the Ni(100) surface.^{25,28} The dependence of the surface-CO interactions on the nature of the metal surface will be the subject of subsequent Hamilton population studies.

A. A model for CO chemisorption on Ni(100)

Following our earlier work,²⁸ the Ni(100) surface is modeled by a four-layer Ni slab with a $\theta = \frac{1}{2}$ coverage of carbon monoxide on one face of the slab, as illustrated in Fig. 4. All geometrical and computational parameters were taken from our previous work,²⁸ and are detailed in the Appendix.

Before attempting an analysis of surface-CO interactions an appropriate energy partitioning scheme must be chosen. A Crystal Fragment Hamilton Population (CFHP) analysis [Eqs. (68)–(70)], based on the crystal fragmentation illustrated in Fig. 5, reduces the problem of analyzing slab-CO interactions to one of analyzing Ni surface layer-CO interactions. “Bulk” Ni-CO interactions account for a mere 0.5% of the total slab-CO interaction.

Figure 6 summarizes the CFHP energy partitioning, for the “bulk”-surface-CO crystal fragmentation given in Fig. 5. It is instructive to note that “chemically relevant energy changes,” such as heats of reaction and adsorption, in general are a minor component of the total energy of the system. The crystal fragment energy partitioning of Fig. 6 illustrates this, Ni slab-CO interactions accounting for a mere 1.6% of the total energy. This was also true in the fragment energy

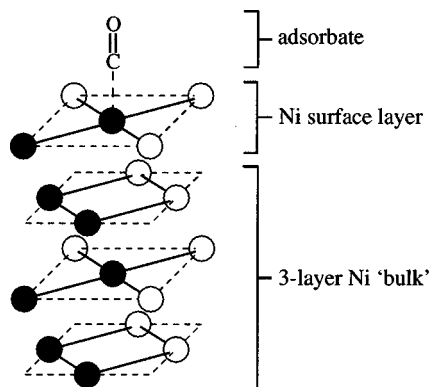


FIG. 5. The crystal fragmentation scheme within the supercell defining the four-layer $c(2 \times 2)$ -CO/Ni(100) slab. Ni atoms belonging to the supercell are shown in black.

partitioning for ethane presented earlier — the strong interaction between two methyl fragments accounted for only 4.7% of the total electronic energy.

B. The role of the CO 4σ orbital in surface-CO bonding

In order to assess the relative bonding role of the various CO molecular orbitals in surface-adsorbate binding, it is necessary to compute the surface-CO COHP's in a crystal fragment orbital basis. The crystal fragmentation of Fig. 5 is used. At this point one can ask: "How (spatially) localized is the CO-surface interaction?" It will prove instructive to address this question before proceeding further with an analysis of surface-CO interactions.

Let us begin by defining "surface-CO interaction" within a Hamilton population energy partitioning. Following the CFHP energy partitioning of Eq. (70) for a CFO basis, the total interaction between the Ni surface and the $c(2 \times 2)$ layer of chemisorbed CO molecules is given by

$$E_{\text{Ni-CO}} = \text{CFHP}_{\text{CO-Ni}}^{\text{FMO}}(\mathbf{0}) + \sum_{\mathbf{R} \in \mathbf{R}^+} \{ \text{CFHP}_{\text{CO-Ni}}^{\text{FMO}}(\mathbf{R}) + \text{CFHP}_{\text{Ni-CO}}^{\text{FMO}}(\mathbf{R}) \}. \quad (71)$$

Equation (71) explicitly partitions the $c(2 \times 2)$ CO-Ni(100) interaction into the interaction between the Ni surface atoms

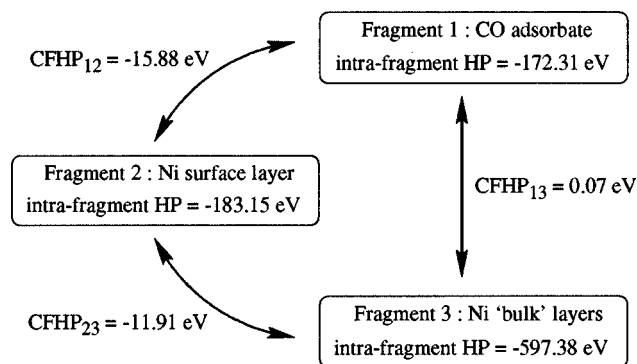


FIG. 6. CFHP energy partitioning for $c(2 \times 2)$ -CO/Ni(100) according to the crystal fragmentation scheme given in Fig. 5.

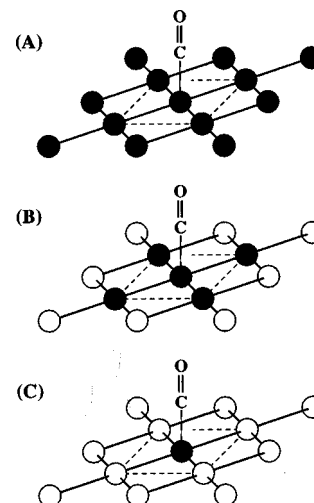


FIG. 7. Surface-CO bonding models for $c(2 \times 2)$ -CO/Ni(100). **Model (A)**, the chemisorbed $c(2 \times 2)$ CO layer interacting with the full Ni(100) surface layer. Only the CO molecule in the home unit cell is shown. **Model (B)**, a chemisorbed CO molecule interacting with the nearest and next nearest neighbor Ni atoms (Ni_α and Ni_β 's, respectively). **Model (C)**, a single chemisorbed CO molecule interacting with the single nearest neighbor atom of the surface (Ni_α). The $p(2 \times 2)R45^\circ$ supercell is shown dashed.

and the CO molecule in the home unit cell, $\text{CFHP}_{\text{CO-Ni}}^{\text{FMO}}(\mathbf{0})$, intercell interactions between CO in the home cell and the Ni surface, $\text{CFHP}_{\text{CO-Ni}}^{\text{FMO}}(\mathbf{R})$ and intercell interactions between the Ni surface atoms in the home cell and the $c(2 \times 2)$ CO layer, $\text{CFHP}_{\text{Ni-CO}}^{\text{FMO}}(\mathbf{R})$.

To investigate the Ni surface layer-CO interactions in greater depth consider the 3 surface layer-CO interaction schemes given in Fig. 7, subsequently referred to as surface-CO bonding models A, B, and C.

Model A refers to the interaction between the complete Ni surface layer and the chemisorbed CO layer. Thus the surface-CO interaction calculated using model A, $E_{\text{Ni-CO}}^{\text{A}} = E_{\text{Ni-CO}}$ as defined by Eq. (71).

Models B and C utilize a subdivision of the Ni surface layer into two crystal fragments containing, respectively, those surface Ni atoms directly bonded and not directly bonded to a chemisorbed CO molecule.

The surface-CO interaction for model B is defined by Eq. (72). The interaction has two distinct components, A subset of the chemisorbed CO molecules in the $c(2 \times 2)$ layer interacting with (1) a single Ni surface atom (Ni_α) bound directly to a chemisorbed CO molecule; (2) the four Ni surface atoms (Ni_β 's) adjacent to Ni_α ,

$$E_{\text{Ni-CO}}^{\text{B}} = \text{CFHP}_{\text{CO-Ni}_\alpha}^{\text{FMO}}(\mathbf{0}) + \text{CFHP}_{\text{CO-Ni}_\beta}^{\text{FMO}}(\mathbf{0}) + \sum_{\mathbf{R} \in \mathcal{G}} \{ \text{CFHP}_{\text{CO-Ni}_\beta}^{\text{FMO}}(\mathbf{R}) + \text{CFHP}_{\text{Ni}_\beta\text{-CO}}^{\text{FMO}}(\mathbf{R}) \}. \quad (72)$$

In addition to the home unit cell, the CO molecules and Ni_β 's included in the model are found in supercells $\mathcal{G} = \{ [1,0], [0,1], [1,1] \}$ indexed with respect to supercell vectors ($\mathbf{a} + \mathbf{b}$) and ($\mathbf{b} - \mathbf{a}$). The surface vectors \mathbf{a} and \mathbf{b} are defined in Fig. 4. The final term in Eq. (72) accounts for less than 0.01 eV of surface-CO interaction and is thus dropped from the

TABLE IV. CFHP analysis of surface-CO bonding for the surface-CO bonding models given in Fig. 7. All values are given in units of eV.

CO orbital	Surface-CO bonding model		
	A	B	C
3 σ	0.16	0.17	0.13
4 σ	-2.24	-2.25	-2.31
1 π	0.27	0.26	0.22
5 σ	-8.32	-8.34	-8.06
2 π	-5.71	-5.70	-4.96
6 σ	-0.03	-0.03	-0.03

analysis. Thus the surface-CO interaction in model B is effectively between a single chemisorbed CO molecule of the $c(2\times 2)$ layer and the five closest Ni surface atoms, and is given by Eq. (73),

$$\mathbf{E}_{\text{Ni-CO}}^{\text{B}} = \text{CFHP}_{\text{CO-Ni}_\alpha}^{\text{FMO}}(\mathbf{0}) + \text{CFHP}_{\text{CO-Ni}_\beta}^{\text{FMO}}(\mathbf{0}) + \sum_{\mathbf{R} \in \mathbf{G}} \text{CFHP}_{\text{CO-Ni}_\beta}^{\text{FMO}}(\mathbf{R}). \quad (73)$$

Finally, surface-CO bonding model C describes the interaction between a chemisorbed CO molecule and the single, nearest neighbor Ni surface atom. Thus the surface-CO interaction calculated using model C is given by the first term in Eq. (73). It should be noted that surface-CO bonding model C is distinct from a linear triatomic Ni-CO ‘‘cluster’’ bonding model, for in the case of model C, the nickel valence orbitals are dispersed throughout the s , p , and d bands of the Ni slab. Metal-carbonyl bonding on surfaces and in molecular species will be contrasted in a later section.

Table IV summarizes the contributions of the CO molecular orbitals to surface-CO interaction for bonding models A, B, and C. An orbital-by-orbital comparison of the CO molecular orbital contributions to surface-CO bonding in models A, B, and C reveals that only the CO 5 σ and 2 π^* contributions vary significantly between models A, B, and C. The ~ 0.25 eV reduction in CO(5 σ)-surface interaction on going from a completely delocalized bonding picture (model A) to a local bonding picture (model C) corresponds to a reduction of $\sim 2\%$ in the magnitude of surface-CO σ interactions. The corresponding change in surface-CO π interac-

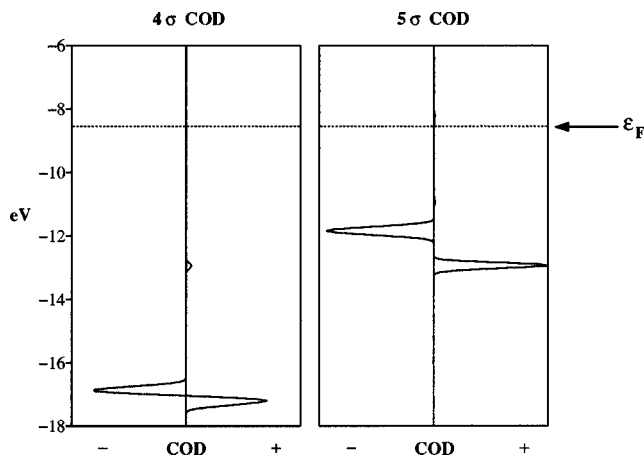


FIG. 8. The crystal orbital displacement (COD) curves for the CO 4 σ and 5 σ orbitals. COD=DOS[$c(2\times 2)$ -CO/Ni(100)]-DOS[$c(2\times 2)$ -CO].

tions is somewhat more substantial at $\sim 13\%$. On the basis of this modest decrease in surface-CO σ interactions, we conclude that surface-CO σ interactions can be modeled adequately by a localized surface-CO bonding model such as model C.

At this point it is convenient to introduce the concept of a ‘‘crystal orbital displacement (COD)’’ developed previously by Ruiz, Alvarez, and co-workers.²⁹ COD is defined as the energy-resolved change in the crystal density of states resulting from a structural change. The COD can be partitioned orbital-by-orbital or FMO-by-FMO.

In this work we are interested in the changes in electronic structure on adsorbing CO on the Ni(100) surface. Consider the CO 4 σ molecular orbital. The 4 σ COD is defined as the difference between the 4 σ DOS in the $c(2\times 2)$ -CO/Ni(100) chemisorption system and the 4 σ DOS for the $c(2\times 2)$ CO array in the absence of the Ni(100) surface. We define our 4 σ COD in such a way that a positive contribution to the COD represents a buildup of 4 σ DOS on binding CO to the nickel surface. The 4 σ COD is given in Fig. 8.

Note the positive-negative feature in the 4 σ COD at ~ -17 eV in Fig. 8. This is the COD signature of a stabilizing orbital interaction — the 4 σ DOS in the composite system appears at lower energy. A much smaller feature can be

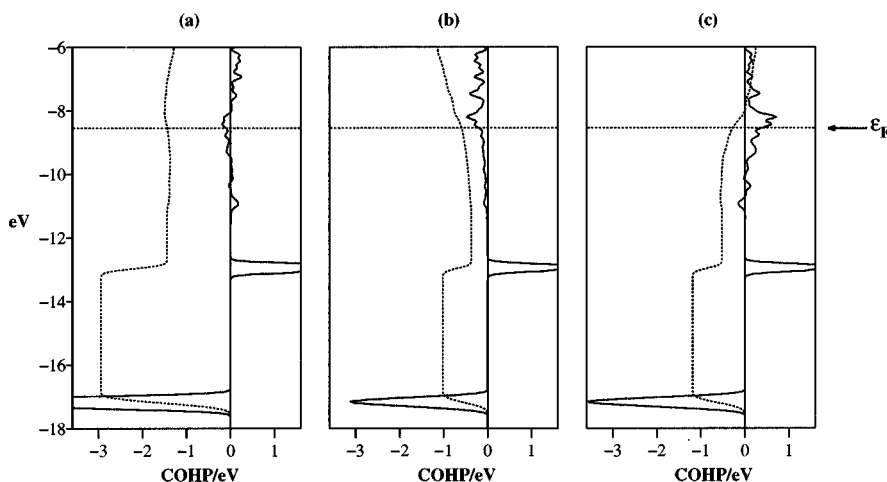


FIG. 9. Surface-4 σ COHP plots for surface (a) s , (b) p_σ , and (c) d_σ bands within bonding model C. COHP integrations are represented by dotted lines.

TABLE V. Surface s , p_σ , and d_σ -CO(4σ) COHP's for surface-CO bonding model C, along with the corresponding partial surface-CO 4σ COHP's obtained by integrating through the 5σ band only (approximately -12 eV through -14 eV).

Surface band	Surface- 4σ COHP/eV	
	Total COHP	5σ band integration
s	-1.43	1.50
p_σ	-0.58	0.65
d_σ	-0.30	0.67

seen in the 4σ COD at ~ -13 eV. This feature of the 4σ COD is a result of 4σ mixing into the CO 5σ -dominated band for the composite system, which is itself identified as the positive component of the positive-negative 5σ COD feature at ~ -13 eV shown in Fig. 8. A significant mixing of the CO 4σ and 5σ states for the CO/Pt(111) chemisorption system was recently noted in the density functional study of Aizawa and Tsuneyuki.²⁷

In order to assess the character and magnitude of the surface- 4σ interaction, the surface s , p_σ , and d_σ -CO 4σ COHP's were calculated and are shown in Fig. 9.

As can be seen from Fig. 9 there are two major contributors to each of the surface s , p_σ , and d_σ - 4σ COHP's. The principal contributor is the stabilizing surface- 4σ interaction described by the positive-negative 4σ COD feature at ~ -17 eV, which results in relatively large negative contributions to the COHP integration curves in Fig. 9.

The much less significant 4σ COD feature — a small positive COD at ~ -13 eV — also contributes significantly to the surface- 4σ COHP, this time in a destabilizing way as indicated by the positive contributions to the surface s , p_σ , and d_σ - 4σ COHP's in Fig. 9.

The total surface- 4σ COHP (within bonding model C) is defined as the sum of the surface s , p_σ , and d_σ - 4σ COHP's. The magnitude of each is given by the energy (on the horizontal axis) corresponding to the point of intersection of the COHP integration curve and the Fermi level — indicated by the dashed line in Fig. 9.

The reduction in surface- 4σ bonding due to 4σ mixing into the higher lying 5σ band is obtained by integrating the surface s , p_σ , and d_σ - 4σ COHP's over the energy range containing the 5σ band (approximately -12 eV through -14 eV). The Ni s , p , and d contributions to the total surface- 4σ COHP are given in Table V along with the “ 5σ band integrations” — the surface s , p_σ , and d_σ - 4σ COHP contributions for the energy range spanning the 5σ band.

Clearly if estimates of surface-adsorbate bonding energy are required, a bonding model must explicitly include the 4σ CO orbital. The 4σ orbital accounts for $\sim 22\%$ of the total sigma bonding contribution to surface-CO binding (see Table IV). An orbital occupation analysis of σ CO-metal charge donation and metal- $2\pi^*$ backdonation (see Table VI) suggests that metal- $2\pi^*$ backdonation dominates, resulting in a flow of charge from the Ni surface to the adsorbed CO molecules. On adsorbing CO on the Ni surface, CO acquires a net charge of $-0.25 e$, and the charge on the Ni surface atoms bonded directly to adsorbed CO is reduced by $0.79 e$, resulting in a net charge of $+0.63 e$. The charge on the Ni

TABLE VI. Orbital occupation analysis for $c(2\times 2)$ -CO/Ni(100).

Changes in CO orbital occupations		
$\Delta 4\sigma$		-0.12
$\Delta 5\sigma$		-0.38
$\Delta 2\pi$		0.75
Changes in surface atom orbital occupations		
	Ni bound to CO	Ni without CO
Δs	-0.04	-0.03
Δp_σ	0.17	0.01
Δp_π	0.04	0.02
Δd_σ	-0.50	0.00
Δd_π	-0.48	-0.02
Δd_δ	0.02	-0.07

surface atoms not directly bonded to adsorbed CO decreases marginally from $-0.17 e$ to $-0.06 e$. The balance of the charge lost by the Ni surface atoms is accommodated in the underlying Ni “bulk” layers.

Despite being responsible for $\sim 25\%$ of σ CO-metal charge donation, the 4σ orbital does not appreciably reduce the significance of metal- $2\pi^*$ backdonation. Thus we think the frontier orbital surface-CO interaction model introduced by Blyholder²³ provides a reasonable model, if one focuses on net surface to CO electron flow. However, even within an extended Hückel framework, application of the Blyholder model in a quantitative fashion will result in an overestimate of charge flow from the surface to the adsorbed CO molecules, and will underestimate surface-CO binding by $\sim 15\%$. A four orbital basis on CO, consisting of the 4σ , 5σ , and $2\pi^*$ MO's is needed to adequately model surface-CO interactions. Figure 10 schematically illustrates the interaction between the Ni(100) surface and a $c(2\times 2)$ adsorbed layer of CO molecules for the proposed four orbital CO basis.

C. A role for the CO(1π) orbitals in surface-CO bonding?

Surface-CO bonding models utilizing a 4σ , 1π , 5σ , and $2\pi^*$ basis on CO were recently proposed by Nilsson *et al.*^{5,30} on the basis of an x-ray emission study of surface-adsorbate interactions in the CO/Ni(100) and N₂/Ni(100) chemisorption systems. Selective probing of the carbon and oxygen x-ray emission spectra — which are dominated by the $2p \rightarrow 1s$ transition, resulted in previously unidentified features in the “ d -band region” just below the Fermi level. A “symmetry resolved” x-ray analysis — which permits resolution of σ and π spectral components resulting from $2p \rightarrow 1s$ transitions from p -states directed normal and parallel to the metal surface respectively, revealed that the additional x-ray features in the d -band region were of “ π symmetry.” Further, carbon and oxygen localized features — which are to a large extent mutually exclusive — were observed in the d -band region with maxima at ~ 2 eV and ~ 5 eV below the Fermi level respectively. Nilsson *et al.*^{5,30} proposed $1\pi-2\pi^*$ mixing to account for these features.

In our analysis (see Table IV), we do not observe a significant bonding role for the CO(1π) orbitals. However,

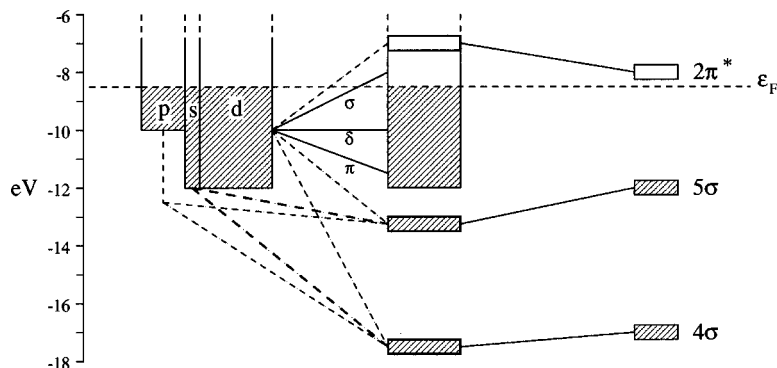


FIG. 10. Surface-CO interaction diagram for the $c(2 \times 2)$ -CO/Ni(100) chemisorption system. Major and minor bonding contributions are denoted by solid and dashed lines, respectively.

we will take this opportunity to investigate the extent of 1π - $2\pi^*$ mixing for the CO/Ni(100) chemisorption system.

Consider the CO(1π) and CO($2\pi^*$)-surface COHP's given in Fig. 11. The surface-CO(1π) COHP has two noteworthy features: (1) A stabilizing surface- 1π interaction at ~ -14 eV worth ~ -0.13 eV, and (2) Metal d_{π} -CO(1π) destabilizing interactions dispersed throughout the d -band region (~ -12 eV through -8 eV) worth ~ 0.35 eV.

What do the states with π symmetry in the d -band region look like? From the surface-CO bonding schematic, Fig. 10, we see that Ni-CO($2\pi^*$) bonding interactions give rise to the π states in the d -band region. The Ni-CO($2\pi^*$) bonding states can be clearly identified in the d -band region of the surface-CO($2\pi^*$) COHP (Fig. 11). The Ni-CO($2\pi^*$) antibonding interactions shown schematically in Fig. 10 can also be clearly distinguished in the surface-CO($2\pi^*$) COHP at ~ -7 eV.

To address the question of 1π - $2\pi^*$ mixing we must focus on the states of π symmetry in the d -band region; these are surface-CO states with 1π and $2\pi^*$ contributions. As we have just noted, these states are formally bonding with respect to the nickel surface and the CO($2\pi^*$) levels. The relative magnitudes of the surface-CO(1π) and surface-CO($2\pi^*$) COHP's shown in Fig. 11 indicate that surface-CO(1π) interactions are an order of magnitude weaker than surface-CO($2\pi^*$) interactions; thus we choose

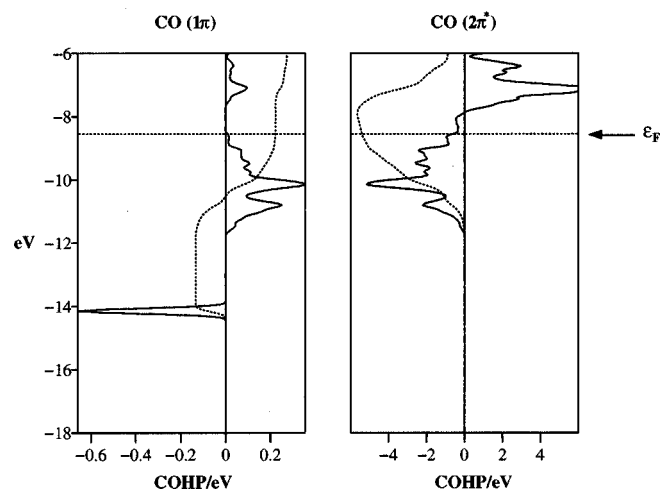


FIG. 11. Surface-CO(1π) and surface-CO($2\pi^*$) COHP's for the CO/Ni(100) chemisorption system.

to consider the surface- 1π interaction a perturbation on the surface- $2\pi^*$ interaction. Hence we arrive at the three band mixing model of surface-CO π interactions illustrated schematically in Fig. 12.

The three band mixing model results in two CO dominated bands — the low-lying 1π band, which is Ni-CO bonding and the high-lying, Ni-CO antibonding, $2\pi^*$ band. The Ni-CO($2\pi^*$) bonding states we find in the d -band region are predominantly metal in character. The extent of 1π - $2\pi^*$ mixing in these mainly metal d -bands was assessed by analyzing contour plots of the π bands. A small carbon to oxygen ‘‘polarization’’ was noted on moving down through the π bands in the d -band region, as illustrated schematically in Fig. 12.

As noted by Nilsson³⁰ the three orbital interaction scheme is a general feature of orbital interactions, nothing specific to this problem. The archetypal case might be the construction of the π orbitals of the allyl system from those of ethylene and a p -orbital on a third carbon atom, illustrated in Fig. 13.

The lowest orbital (π) mixes into itself the p -orbital in a bonding way. The highest orbital (π^*) is destabilized by out-of-phase mixing with the p -orbital. The p -orbital mixes into itself both π (in an antibonding way) and π^* (in a bonding way). The energy of this middle orbital is unchanged to a first approximation, but its shape (polarization) is dramatically affected, in a predictable way.^{16,31}

In the surface case the role of π is played by 1π of CO, the role of π^* by $2\pi^*$ and the role of the p -orbital by a surface Ni d orbital. The various orbitals are spread out into bands of course, and the surface d band in particular is broad. The mixing of 1π and $2\pi^*$ into the d band is variable, but

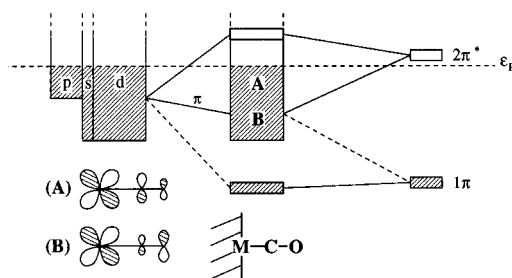


FIG. 12. A three band mixing model of surface-CO π interactions for the CO/Ni(100) chemisorption system.

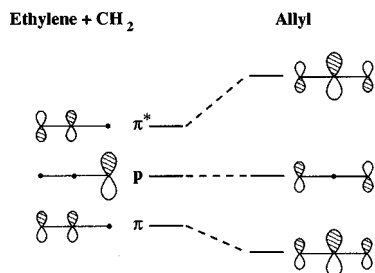


FIG. 13. A three orbital mixing model for the formation of the allyl π molecular orbitals from those of ethylene and the unhybridized p -orbital of CH_2 .

can be understood in detail. Mixing of the 1π (which is concentrated on the oxygen atom of CO) into the d band increases towards the bottom of the d band and mixing of the $2\pi^*$ (concentrated on carbon) increases towards the top of the d band.

Could this carbon to oxygen polarization on descending through the d -band be responsible for the carbon and oxygen centered π features noted by Nilsson *et al.*?⁵ The carbon and oxygen centered π features observed by Nilsson *et al.* in the d -band region are presumably a result of $2p \rightarrow 1s$ transitions. Thus on projecting the $\text{C}(p_\pi)$ and $\text{O}(p_\pi)$ DOS we expect to observe essentially mutual exclusivity in the d -band region. The $\text{C}(p_\pi)$ and $\text{O}(p_\pi)$ projected DOS curves are given in Fig. 14.

Clearly, on examination of Fig. 14, we cannot partition the d -band region into $\text{C}(p_\pi)$ and $\text{O}(p_\pi)$ dominated blocks. Thus we conclude that, based on the results of our extended Hückel treatment of surface-CO interactions, $1\pi-2\pi^*$ mixing is neither significant, nor is it responsible for the carbon and oxygen localized π features observed by Nilsson *et al.* in the d -band region.

D. Nickel s , p , and d band contributions to CO/Ni(100) bonding

The relative importance of metal s , p , and d bands in binding CO to transition metal surfaces is not, in general, well defined. A previous extended Hückel study from our group²⁵ on the CO/M(111) ($M=\text{Ni}, \text{Pd}, \text{Pt}$) chemisorption systems concluded that for CO adsorption at the on-top site, interaction of the CO 5σ band with the metal s and p_σ bands

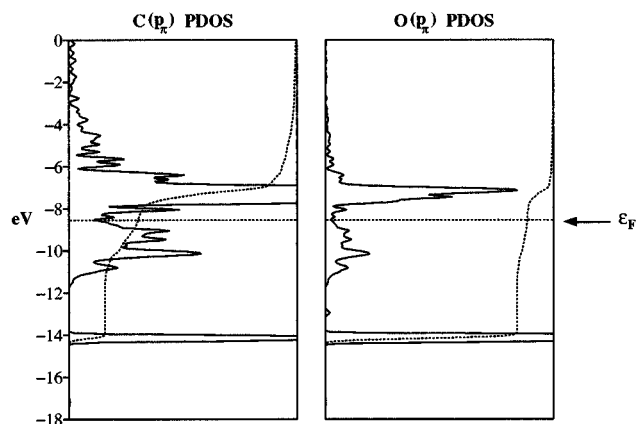


FIG. 14. Projected DOS curves for the carbon and oxygen p_π basis functions; p orbitals oriented parallel to the Ni surface.

dominates. The significance of the CO 5σ band for surface-CO interactions is clear from Table IV.

The nickel s , p_σ , and d_σ COD curves provide a visual measure of the extent to which the surface s , p_σ , and d_σ states mix into the CO 4σ and 5σ dominated bands at ~ -17 eV and ~ -13 eV illustrated in the schematic surface-CO bonding scheme of Fig. 10. We define the nickel s , p_σ , and d_σ COD's to be the nickel s , p_σ , and d_σ projections of the total DOS difference between the $c(2 \times 2)$ -CO/Ni(100) chemisorption system and the clean Ni(100) slab. The nickel s , p_σ , and d_σ COD's are given in Fig. 15. The nickel s , p_σ , and d_σ contributions to the predominantly CO 4σ and 5σ bands at ~ -17 eV and ~ -13 eV can be clearly seen.

Some additional, qualitative information about the nature of the surface-CO interaction can be directly derived from the COD integrations in Fig. 15. The principal feature of interest is the reduction in d_σ DOS below the Fermi level on binding CO to the surface. This is due to d_σ -CO σ interaction, which results in the surface d_σ band being pushed partially above the Fermi level.

Table VII summarizes surface-CO 4σ , 5σ , and $2\pi^*$ interactions for surface-CO bonding model A with respect to a Ni $\{s, p_\sigma, p_\pi, d_\sigma, d_\pi\}$ basis. The metal d_δ orbitals are omitted from the analysis since they account for less than 0.005% (~ 0.05 eV) of the total surface-CO $\{4\sigma, 5\sigma, 2\pi^*\}$ interaction.

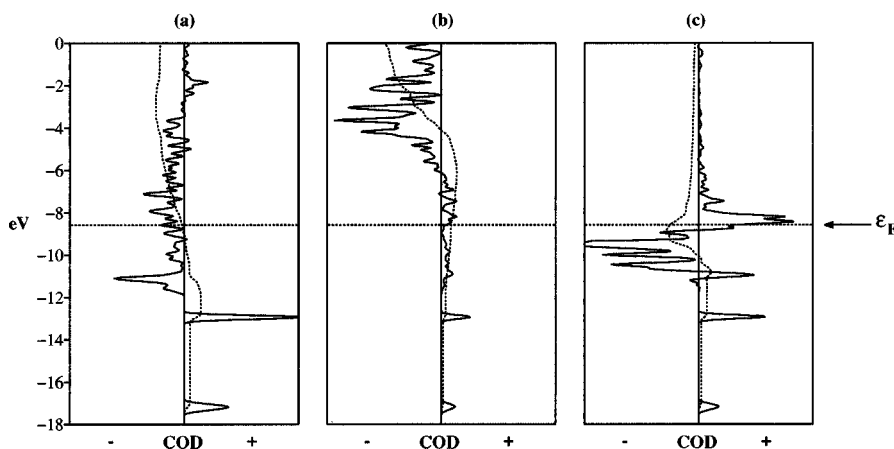


FIG. 15. Nickel (a) s , (b) p_σ and (c) d_σ COD's for surface-CO bonding model C. The dotted lines correspond to COD integrations.

TABLE VII. Surface s , p , and d band contributions to surface-CO $\{4\sigma, 5\sigma, 2\pi^*\}$ interactions for surface-adsorbate bonding model A. All values are given in units of eV.

Nickel band	CO orbital		
	4σ	5σ	2π
s	-1.43	-4.19	-0.38
p_σ	-0.58	-2.58	-0.08
d_σ	-0.30	-1.47	-0.02
p_π	0.04	0.00	-0.56
d_π	0.00	-0.04	-4.50

Clearly metal s , p , and d bands all contribute significantly to surface-CO bonding. That bonding, in the case of CO chemisorbed on-top on the Ni(100) surface, may best be described as CO 4σ and 5σ orbitals interacting with an sp dominated spd hybrid metal band, thus refining the CO (5σ)-metal d_σ forward donation proposed by the Blyholder model.²³ Surface-CO π backdonation is quite well described by the metal d_π -CO($2\pi^*$) Blyholder backdonation model, metal d_π states accounting for $\sim 80\%$ of the surface-CO ($2\pi^*$) interaction.

XIV. A SURFACE-MOLECULE BINDING ANALOGY

In this section an analogy will be drawn between nickel-CO binding in the $c(2\times 2)$ -CO/Ni(100) chemisorption system and the hypothetical 18 electron complex $[\text{H}_5\text{NiCO}]^-$. Such surface-molecule bonding analogies allow for the construction of logical bridges between seemingly widely differing subject areas such as surface science and organometallic chemistry. This system in particular has been used in this context earlier.² As will be shown in this section, the analogy between CO bonding to the Ni(100) surface and Ni-CO bonding in $[\text{H}_5\text{NiCO}]^-$ is by no means just a theoretical construct — many qualitative and quantitative aspects of Ni-CO bonding in $[\text{H}_5\text{NiCO}]^-$ are reproduced for CO chemisorbed on the Ni(100) surface.

We begin the discussion of Ni-CO bonding in $[\text{H}_5\text{NiCO}]^-$ by examining the interaction between the square

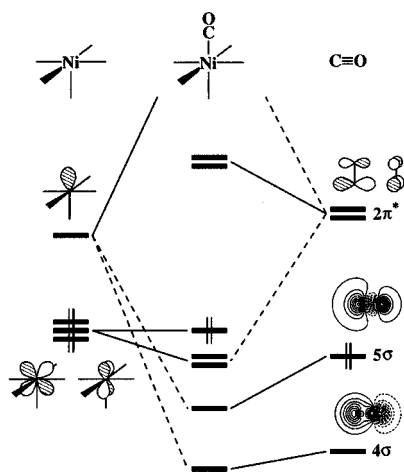


FIG. 16. Principal orbital interactions between the $[\text{H}_5\text{Ni}]^-$ and CO fragments in $[\text{H}_5\text{NiCO}]^-$.

TABLE VIII. Orbital occupation analysis for $[\text{H}_5\text{NiCO}]^-$.

Changes in CO orbital occupations			
	$\Delta 4\sigma$		-0.12
	$\Delta 5\sigma$		-0.41
	$\Delta 2\pi$		0.52
Changes in Ni orbital occupations			
Δs	-0.02	Δd_σ	0.34
Δp_σ	0.20	Δd_π	-0.48
Δp_π	-0.02	Δd_δ	0.00

pyramidal $[\text{NiH}_5]^-$ fragment and the carbonyl ligand. The principal interactions between the fragments are illustrated schematically in Fig. 16.

As shown in Fig. 16, σ interaction between the $[\text{NiH}_5]^-$ and CO fragments is dominated by the LUMO on $[\text{NiH}_5]^-$ — a low-lying σ acceptor function. π interaction between the fragments is dominated by Ni(d_π)-CO($2\pi^*$) interactions, in agreement with the conclusions of previous discussions on π interactions between the Ni(100) surface and chemisorbed CO.

An analysis of the changes in CO and Ni orbital occupations on forming $[\text{H}_5\text{NiCO}]^-$ from $[\text{NiH}_5]^-$ and CO is summarized in Table VIII and largely parallels the analysis for CO on Ni(100) given in Table VI.

There exists, however, one significant difference between the orbital occupation analyses for $[\text{H}_5\text{NiCO}]^-$ and CO on Ni(100). As can be seen from Fig. 15, the Ni d_σ band for the Ni(100) surface (which is filled in the absence of CO chemisorbed on the surface), is partially raised above the Fermi level on binding CO to the surface. Thus the occupancy of the Ni d_σ band is reduced by 0.5 electrons on binding CO to the Ni surface. In contrast, the occupancy of the Ni d_σ state increases on forming $[\text{H}_5\text{NiCO}]^-$ from $[\text{NiH}_5]^-$ and CO fragments. In $[\text{NiH}_5]^-$ the Ni d_σ orbital is concentrated in the LUMO (see Fig. 16). Thus the occupancy of the Ni d_σ orbital increases via mixing of the LUMO on the $[\text{NiH}_5]^-$ fragment with both the CO 4σ and 5σ orbitals.

Table IX contrasts the contributions of the CO orbitals to Ni-CO interactions for both molecular $[\text{H}_5\text{NiCO}]^-$ and CO chemisorbed on a Ni(100) surface.

Clearly, the relative contributions of the CO orbitals to Ni-CO interaction in molecular $[\text{H}_5\text{NiCO}]^-$ parallel those for CO chemisorbed on the Ni(100) surface, as measured by the fragment Hamilton populations. Table X details the con-

TABLE IX. CO orbital contributions to Ni-CO interaction for molecular $[\text{H}_5\text{NiCO}]^-$ and $c(2\times 2)$ -CO/Ni(100) within surface-CO bonding model C.

CO orbital	Ni-CO FHP/eV	
	CO/Ni(100)	$[\text{H}_5\text{NiCO}]^-$
3σ	0.13	0.14
4σ	-2.31	-2.13
1π	0.22	0.28
5σ	-8.06	-7.78
2π	-4.96	-4.47
6σ	-0.03	-0.02

TABLE X. Ni s , p , and d band contributions to Ni–CO $\{4\sigma, 5\sigma, 2\pi^*\}$ interactions for $[\text{H}_5\text{NiCO}]^-$. All values are given in units of eV.

Nickel orbital	CO orbital		
	4σ	5σ	2π
s	-0.33	-1.86	0.00
p_σ	-0.83	-3.13	0.00
d_σ	-0.98	-2.78	0.00
p_π	0.00	0.00	-0.11
d_π	0.00	0.00	-4.35

tributions of the Ni s , p_σ , d_σ , p_π , and d_π orbitals to Ni–CO bonding in $[\text{H}_5\text{NiCO}]^-$. Comparison of the relative Ni s , p_σ , and d_σ state contributions to Ni–CO (4σ , 5σ) bonding in $[\text{H}_5\text{NiCO}]^-$ with those given in Table VII for CO on Ni(100) reveals a reduction in the Ni(s) contribution to Ni–CO (4σ , 5σ) bonding in $[\text{H}_5\text{NiCO}]^-$ by approximately 60% with respect to CO chemisorbed on Ni(100). Further, the Ni(d_σ) contribution to Ni–CO bonding in $[\text{H}_5\text{NiCO}]^-$ is increased with respect to CO on Ni(100) by approximately 50%.

The changes in Ni s , p_σ , and d_σ contributions to Ni–CO (4σ , 5σ) bonding can be rationalized by contrasting the Ni s , p_σ , and d_σ molecular orbital displacements (MOD's) – the molecular analog of COD, for the formation of $[\text{H}_5\text{NiCO}]^-$ from $[\text{NiH}_5]^-$ and CO fragments with those for CO on Ni(100) given in Fig. 15. The Ni s , p_σ , and d_σ contributions to the CO 4σ and 5σ bands at ~ -17 eV and ~ -13 eV, respectively, for CO on Ni(100) can be clearly distinguished in Fig. 15. The corresponding Ni s , p_σ , and d_σ MOD's for the formation of $[\text{H}_5\text{NiCO}]^-$ from $[\text{NiH}_5]^-$ and CO fragments are given in Fig. 17.

A FMO-by-FMO decomposition of the total $[\text{H}_5\text{NiCO}]^-$ DOS for the fragmentation into $[\text{NiH}_5]^-$ and CO fragments (not shown) reveals that the CO 5σ orbital is concentrated in a molecular state at ~ -13 eV (state II in Fig. 17). The CO 4σ orbital is distributed approximately evenly between two molecular states at ~ -16 eV and ~ -18 eV resulting from the interaction of the totally symmetric combination of nickel and hydrogen s orbitals on the $[\text{NiH}_5]^-$ fragment (FMO A in Fig. 17) with the 4σ CO orbital. The filled 4σ state at ~ -16 eV, which is formally antibonding with respect to the $[\text{NiH}_5]^-$ and CO fragments, is responsible for

the reduction in the Ni(s) component of Ni–CO(4σ) interaction by ~ 1.1 eV with respect to the -1.43 eV Ni(s)– 4σ COHP for CO on Ni(100).

Despite a significant reduction in Ni(s)–CO(4σ) interaction, the majority ($\sim 66\%$; ~ 2.3 eV) of the reduction in Ni(s)–CO σ bonding is attributable to the CO 5σ orbital. Ni–CO σ interactions in $[\text{H}_5\text{NiCO}]^-$ are dominated by the interaction of the 5σ CO orbital with the LUMO for the $[\text{NiH}_5]^-$ fragment — a low-lying σ acceptor function (see Fig. 16). The LUMO of the $[\text{NiH}_5]^-$ fragment is essentially d_σ in character with a minor p_σ contribution (p_σ : d_σ ratio $\sim 1:5$). The lack of Ni(s) participation in Ni–CO(5σ) interaction for $[\text{H}_5\text{NiCO}]^-$ is in marked contrast to the case of CO chemisorbed on the Ni(100) surface and is the primary factor behind the reduction in the Ni(s) component of Ni–CO σ bonding. A comparison of the Ni p_σ and d_σ contributions to Ni–CO(4σ) and Ni–CO(5σ) bonding for CO/Ni(100) and $[\text{H}_5\text{NiCO}]^-$ (Tables VII and X, respectively) indicates that Ni–CO(5σ) interaction also accounts for 66% of the increase in Ni(p_σ , d_σ)–CO interaction for $[\text{H}_5\text{NiCO}]^-$ over CO/Ni(100). The buildup of Ni p_σ and d_σ DOS resulting from the Ni–CO(5σ) interaction in $[\text{H}_5\text{NiCO}]^-$ can be clearly seen in the CO 5σ -dominated molecular state at ~ -13 eV (II) in Fig. 17.

XV. CONCLUSIONS

Hamilton population and overlap population analyses are proposed as complementary tools for analysis of chemical bonding in both molecular and extended structures of 1, 2, or 3 dimensions. The electron partitioning of the Mulliken overlap population analysis — which focuses on a partitioning of electrons between the atomic centers defining the system, is recast in an “atom-bond” (or “on-site,” “off-site”) format. Individual overlap populations are assigned to either a specific atom or to the “bond” between a pair of atoms in the molecule or unit cell.

A Hamilton population partitioning of the total electronic energy has been shown to correspond to an “energy-weighted” overlap population analysis of electron distribution. Hence when the Mulliken overlap population analysis is recast in the aforementioned atom-bond format, chemically intuitive atom and fragment based energy partitioning

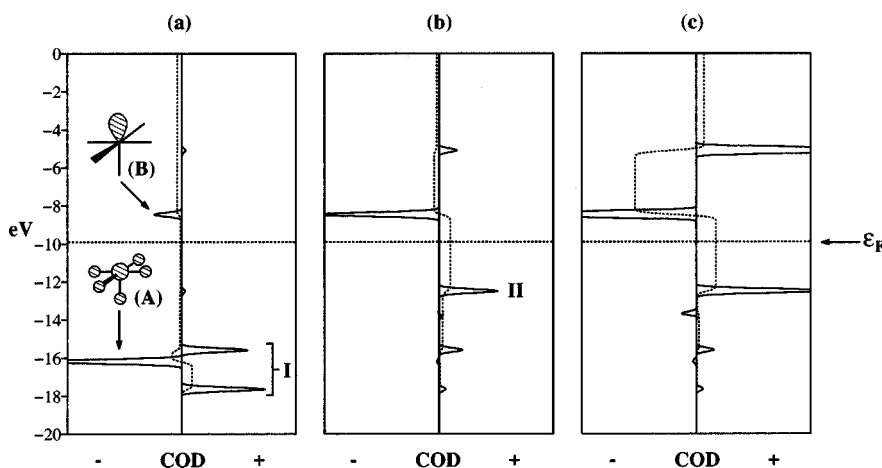


FIG. 17. Ni (a) s , (b) p_σ , and (c) d_σ MOD's for the formation of $[\text{H}_5\text{NiCO}]^-$ from $[\text{NiH}_5]^-$ and CO fragments. The Ni contributions to the 4σ (I) and 5σ (II) molecular states are principally derived from the totally symmetric s state A and the pd σ acceptor function B of $[\text{NiH}_5]^-$, respectively. The dotted lines correspond to COD integrations.

TABLE XI. Extended Hückel parameters used in this study.

Atom	Orbital	H_{ii}/eV	ζ_1	ζ_2	c_1	c_2
H	1s	-13.600	1.300			
F	2s	-40.000	2.425			
	2p	-18.100	2.425			
Cl	3s	-26.300	2.183			
	3p	-14.200	1.733			
Br	4s	-22.100	2.588			
	4p	-13.100	2.131			
Pt	6s	-9.077	2.554			
	6p	-5.475	2.554			
	5d	-12.590	6.013	2.696	0.6334	0.5513
Ni	4s	-7.800	2.100			
	4p	-3.700	2.100			
	3d	-9.900	5.750	2.000	0.5683	0.6292
C	2s	-18.200	1.630			
	2p	-9.500	1.630			
O	2s	-29.600	2.270			
	2p	-13.600	2.270			

schemes can be derived and are illustrated in this work for both molecular and extended systems.

The application of Hamilton population analysis to the study of Ni-CO interactions in the $c(2\times 2)$ -CO/Ni(100) chemisorption system serves to illustrate the utility of energy partitioning in addressing aspects of the Ni-CO interaction which are not amenable to overlap population analysis. The use of a surface-adsorbate fragmentation and a fragment crystal orbital basis proved particularly useful. A significant bonding role for the relatively low-lying CO 4σ orbital is proposed, both for CO chemisorbed "on-top" on the Ni(100) surface and for a molecular $[\text{H}_5\text{NiCO}]^-$ model, the discrete analogue of the CO/Ni(100) chemisorption system.

Hamilton population analysis of the Ni s , p , and d band contributions to Ni-CO interaction for CO chemisorbed on the Ni(100) surface results in the σ component of the interaction being described as CO interacting with an sp dominated spd Ni σ band. Thus the metal d_σ -CO σ bonding model proposed by Blyholder²³ for CO chemisorption on transition metal surfaces needs to be modified somewhat.

We suspect that the full utility of Hamilton population analysis as a theoretical tool for analyzing chemical bonding remains to be demonstrated. Further studies utilizing Hamilton population analysis are currently underway in our group include, comparative studies of CO chemisorption on pure and alloyed transition metal surfaces³² and hydrocarbon bonding to platinum surfaces.³³

ACKNOWLEDGMENT

We are grateful to the National Science Foundation for its support of this work by Research Grant No. CHE 94-08455.

APPENDIX

All calculations are of the extended Hückel-type and were performed with the YAeHMOP package.^{34,35} A double ζ expansion was used for the Ni d -orbitals. The extended Hückel parameters used in this study are detailed in Table XI

— the parameters for Ni, C, and O being taken directly from our previous study.²⁸

The bond lengths 0.91 Å, 1.28 Å, and 1.61 Å, respectively, for the hydrogen halides HX (X=F, Cl, Br) were obtained from the CRC Handbook.³⁶ All bond lengths for the study of the $c(2\times 2)$ -CO/Ni(100) chemisorption system were taken from a previous study;²⁸ C-O distance 1.15 Å, Ni-C distance 1.80 Å, and Ni-Ni distance (fcc lattice) 2.49 Å. An inter-slab separation of 10 Å was used to eliminate slab-slab interactions.

A manually generated set of 32 k -points was used to sample the irreducible wedge of the Brillouin zone for the $c(2\times 2)$ -CO/Ni(100) system defined by $0 < k_a \leq (\pi/2)$, $0 < k_b \leq (\pi/2)$, $-(\pi/2) < k_c \leq (\pi/2)$ for a tetragonal $p(2\times 2)R45^\circ$ supercell defined with respect to the in-surface vectors **a** and **b** as illustrated in Fig. 4.

The Ni-C and C-O distances used in the study of $[\text{H}_5\text{NiCO}]^-$ were as for the $c(2\times 2)$ -CO/Ni(100) study. The Ni-H distance of 1.57 Å was calculated to be the sum of the nickel and hydrogen covalent radii obtained from the online Periodic Table webelements.³⁷

- R. Dronskowski and P. E. Blöchl, *J. Phys. Chem.* **97**, 8617 (1993).
- R. Hoffmann, *Solids and Surfaces: A Chemist's View of Bonding in Extended Structures* (VCH, New York, 1988).
- R. Dronskowski, *J. Am. Chem. Soc.* **114**, 7230 (1992).
- J. A. Pople, D. P. Santry, and G. A. Segal, *J. Chem. Phys.* **43**, S129 (1965).
- A. Nilsson, N. Wassdahl, M. Weinelt, O. Karis, T. Wiell, P. Bennich, J. Hasselström, A. Föhlisch, J. Stöhr, and M. Samant, *Appl. Phys. A: Mater. Sci. Process.* **65**, 147 (1997).
- M. Kawai and J. Yoshinobu, *Surf. Sci.* **368**, 239 (1996); **363**, 105 (1996).
- M. Kawai, J. Yoshinobu, and N. Takagi, *Surf. Sci.* **363**, 85 (1996).
- A. Grossmann, W. Erley, and H. Ibach, *Surf. Sci.* **355**, L331 (1996); **330**, L646 (1995).
- J. Yoshinobu, N. Takagi, and M. Kawai, *Phys. Rev. B* **49**, 16670 (1994).
- N. Vasquez, A. Muscat, and R. J. Madix, *Surf. Sci.* **301**, 83 (1994).
- J. Lauterbach, M. Wittmann, and J. Küppers, *Surf. Sci.* **279**, 287 (1992).
- F. Mele, N. Russo, and M. Toscano, *Surf. Sci.* **307**, 113 (1994).
- R. Maruca, T. Kusuma, V. Hicks, and A. Companion, *Surf. Sci.* **236**, 210 (1990).
- J. N. Allison and W. A. Goddard, *Surf. Sci.* **115**, 553 (1982); **110**, L615 (1981).
- (a) R. Hoffmann and W. N. Lipscomb, *J. Chem. Phys.* **36**, 2179 (1962); **36**, 3489 (1962); (b) **37**, 2872 (1963); (c) R. Hoffmann, *ibid.* **39**, 1397 (1963); (d) **40**, 2474 (1964); **40**, 2745 (1964).
- T. A. Albright, J. K. Burdett, and M. -H. Whangbo, *Orbital Interactions in Chemistry* (Wiley-Interscience, 1985).
- B. M. Gimarc, *Molecular Structure and Bonding* (Academic, New York, 1979).
- M. Wolfsberg and L. Helmholz, *J. Chem. Phys.* **20**, 837 (1952).
- M. -H. Whangbo and R. Hoffmann, *J. Chem. Phys.* **68**, 5498 (1978).
- J. H. Ammeter, H. -B. Burgi, J. C. Thibeault, and R. Hoffmann, *J. Am. Chem. Soc.* **100**, 3686 (1978).
- R. S. Mulliken, *J. Chem. Phys.* **23**, 1841 (1955).
- M. -H. Whangbo and R. Hoffmann, *J. Am. Chem. Soc.* **100**, 6093 (1978).
- G. J. Blyholder, *J. Phys. Chem.* **68**, 2772 (1964).
- W. L. Jorgensen and L. Salem, *The Organic Chemist's Book of Orbitals* (Academic, New York, 1973).
- Y. -T. Sung and R. Hoffmann, *J. Phys. Chem.* **95**, 859 (1991).
- P. Hu, D. A. King, M. -H. Lee, and M. C. Payne, *Chem. Phys. Lett.* **246**, 73 (1995).
- H. Aizawa and S. Tsuneyuki, *Surf. Sci.* **399**, L364 (1998).
- Y. -T. Sung and R. Hoffmann, *J. Am. Chem. Soc.* **107**, 578 (1985).
- E. Ruiz, S. Alvarez, R. Hoffmann, and J. Bernstein, *J. Am. Chem. Soc.* **116**, 8207 (1994).
- A. Nilsson, *J. Electron Spectrosc. Relat. Phenom.* **93**, 143 (1998).
- R. Hoffmann, *Acc. Chem. Res.* **4**, 1 (1971).
- W. V. Glassey and R. Hoffmann (in preparation).

³³G. A. Papoian and R. Hoffmann (in preparation).

³⁴G. A. Landrum and W. V. Glassey, bind, version 3.0. bind is distributed as part of the YAeHMOP extended Hückel molecular orbital package and is freely available on the WWW at URL, <http://overlap.chem.cornell.edu:8080/yaehmop.html/>

³⁵G. A. Landrum, viewkel, version 3.0. viewkel is distributed as part of the YAeHMOP extended Hückel molecular orbital package and is freely

available on the WWW at URL, <http://overlap.chem.cornell.edu:8080/yaehmop.html/>

³⁶*CRC Handbook of Chemistry and Physics*, 78th ed. (Chemical Rubber, Cleveland, 1997/1998).

³⁷The online Periodic Table *webelements* by Mark Winter of the University of Sheffield, England, can be found on the WWW at URL, <http://www.shef.ac.uk/chemistry/web-elements/>